NUMERICAL INVESTIGATION OF FLOW AND HEAT TRANSFER CHARACTERISTICS IN RECTANGULAR CHANNELS (AR=4:1) WITH CIRCULAR AND ELLIPTICAL PIN FIN ARRAYS

A Thesis

by

ABHISHEK VELICHALA

NUMERICAL INVESTIGATION OF FLOW AND HEAT TRANSFER

CHARACTERISTICS IN RECTANGULAR CHANNELS (AR=4:1) WITH

CIRCULAR AND ELLIPTICAL PIN FIN ARRAYS

A Thesis

by

ABHISHEK VELICHALA

Submitted to the Office of Graduate Studies of
Texas A&M University
in partial fulfillment of the requirements for the degree of

MASTER OF SCIENCE

Approved by:

Co-Chairs of Committee,	Sai Lau
	Hamn-Ching Chen
Committee Member,	Yassin Hassan
Head of Department,	Dennis O'Neal

May 2011

Major Subject: Mechanical Engineering

ABSTRACT

Numerical Investigation of Flow and Heat Transfer Characteristics in Rectangular

Channels (AR=4:1) with Circular and Elliptical Pin Fin Arrays. (May 2011)

Abhishek Velichala, B.Tech, Indian Institute of Technology, Madras, India

Co–Chairs of Advisory Committee: Dr. Sai Lau
Dr. Hamn-Ching Chen

The objective of current study was to numerically investigate the flow and heat

transfer characteristics in a stationary one pass rectangular channel (AR=4:1) with

circular and elliptical pin fin arrays. Two types of elliptical pin fins (a SEF and

an N fin whose minor axis length is equal to the diameter of the circular fin) were

used. The analysis was performed with an array of six rows of staggered pin fins in

the streamwise direction for Reynolds numbers (Re) of 10,000, 20,000, 30,000, 40,000

and 50,000. 3-D, steady simulations were performed using the low Reynolds number

k-omega SST turbulence model in the FLUENT CFD code. The data predicted by

the current numerical model showed favorable agreement with the experiments in the

validation study. It was observed that SEF array produces minimum pressure loss

and the highest thermal performance. It was also observed that N fin array produces

minimum hot spots and the highest channel averaged Nusselt number ratio values.

To my parents

ACKNOWLEDGMENTS

I would like to thank my co-advisor, Dr. Sai Lau, for giving me total freedom during this journey from the selection of the research objective to the final examination. I am grateful to my other co-advisor, Dr. Hamn-Ching Chen, for providing invaluable input throughout the course of study without which this thesis would have been impossible. I would like to thank Dr. Yassin Hassan for serving on my committee and for being very helpful and supportive.

I would like to thank my parents and roommates who kept me motivated with their constant encouragement. Finally I want to express my appreciation towards Pandora and Youtube for helping me refresh my mind whenever I was too stressed with their extensive collection of music.

TABLE OF CONTENTS

LIST OF TABLES

TABLE   Page

LIST OF FIGURES

CHAPTER I

INTRODUCTION

A. Background

Gas turbines find their applications in various areas, including in aircraft and power generation applications. But the desired operating conditions vary from application to application. The applications in which the inlet temperature is close to the room temperature, the turbines may be capable of operating without reaching unreasonably high temperatures (above 1300ºC). But gas turbines, when utilized as aircraft jet engines and electric generators, the performance improvement results in the higher inlet temperature which could result in the melting, material fatigue or degradation of the turbine material because of the increased heat transfer to the turbines. In order to safely operate the high performance gas turbines, the effective cooling of the elements exposed to high temperature is essential. Research activities which began four decades ago slowly developed into an important research area because of the increased requirement for the cooling of gas turbines in power industry year by year.

Gas turbine cooling techniques can be broadly classified into two categories, external cooling and internal cooling. External cooling is also known as film cooling. It is achieved by discharging the internal coolant air through discrete holes in the turbine walls to provide an insulating coolant film which protects the outer surface of the blade from hot gases. Internal cooling is accomplished by passing the coolant through various enhanced serpentine channels inside the blades and convecting heat from the blade to the coolant. Jet impingement, rib turbulator and pin-fin cooling

---

The journal model is *IEEE Transactions on Automatic Control.*

are the major internal cooling methods. Fig. 1 from Han et al. [1] depicts the common techniques used for cooling gas turbines. Internal cooling of gas turbine blades is enhanced by jet impingement cooling and enhanced convective cooling. Jet impingement cooling is the application of a high velocity coolant stream at the internal surface of turbine blade, thus cooling the airfoil through forced convection. Even though jet impingement has the highest capability to augment the local heat transfer coefficient, due to structural limitations on the rotor blade under high speed rotation, jet impingement cooling is limited only to the leading edge of the turbine blade. Enhanced convective cooling, which is based on the idea of augmenting heat transfer by increasing the cooled surface area and channel flow turbulence is used in the midchord and trailing edge regions of turbine blades. This is accomplished by the usage of rib turbulators, pin fins and dimpled surfaces. Rib turbulators are used on the inner walls of turbine blades in the midchord region, where as pin-fins are used in the blade trailing region because of space constraint and structural integration.

Pin fins help in breaking the flow periodically and reducing the boundary layer thickness, escalating turbulence levels, increasing mixing of the coolant fluid and surface area all of which result in the augmentation of heat transfer. Both Coriolis and rotational buoyancy forces affect the flow and heat transfer distribution within the coolant passage due to rotation. Because of all the factors mentioned above, it is essential to have information on the local heat transfer coefficients in the turbine blade passages. Addition of pin fins increases resistance to the flow of coolant through the channel. Channel pressure loss which determines the power required to pump the coolant through the channel is directly proportional to this flow resistance. An efficient cooling system thus helps in heat transfer enhancement at minimal pressure drop. Several experimental and numerical studies have been conducted through the years for various pin fin shapes, spacing ratios etc., to study the complex flow physics
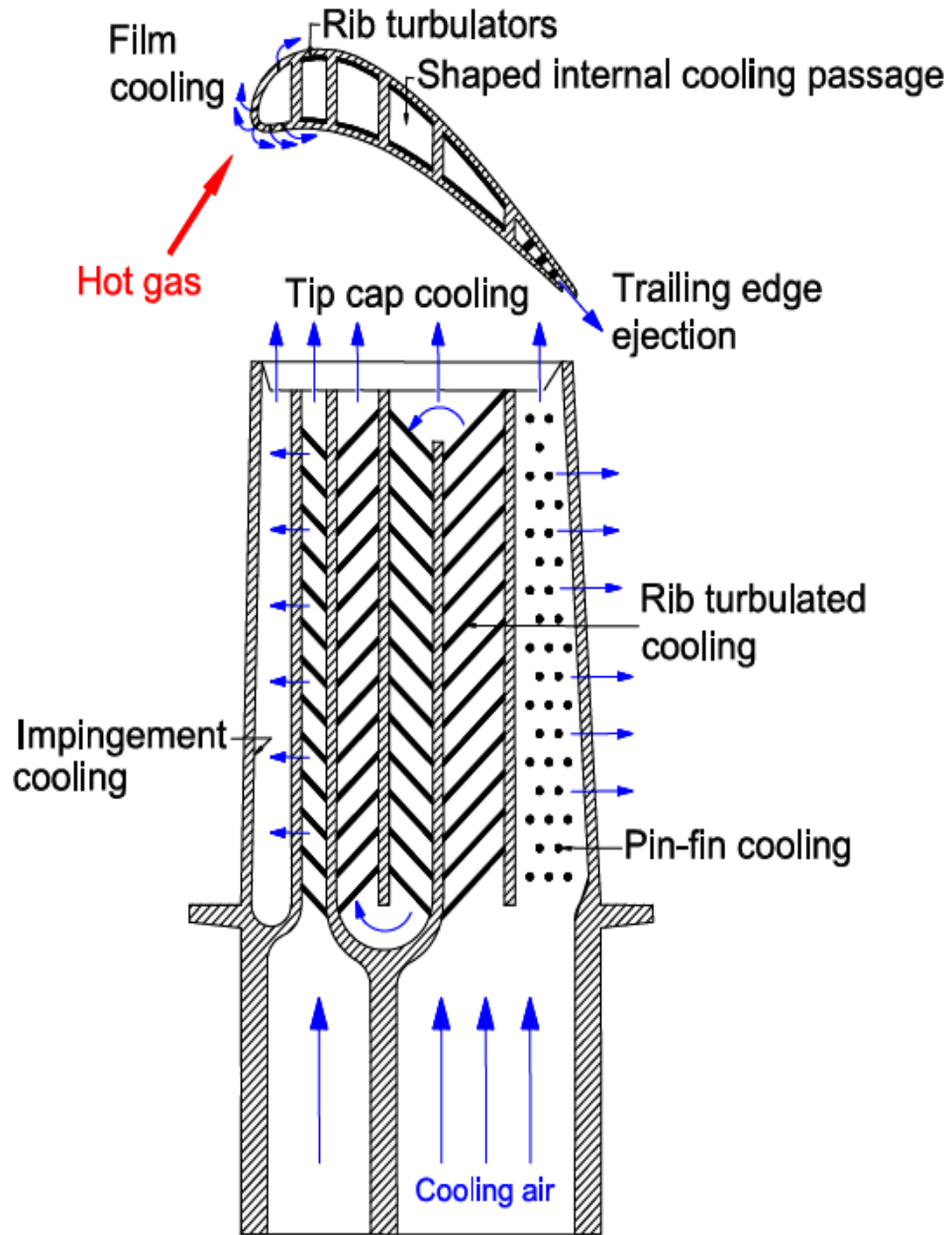
Fig. 1. Cooling techniques used in a modern turbine blade (Han et al. [1])

generated and to come up with an efficient model which will be discussed thoroughly in the literature review section.

B.   Literature Review

1.   Circular pin fins

Vital part of the past pin-fin research has been on the experimental investigation of heat transfer and pressure drop characteristics in circular pin-fin channels for various conformations. Jakob [2] and Grimison [3] conducted some of the early experimental works for long tube array cases where the height-to-diameter ratio is very large. Since the height-to-diameter ratio of pin fins used in the trailing edge of turbines is of the order 1, the results obtained by Jakob [2] and Grimison [3] cannot be applied to them. Vanfossen [4] evaluated heat transfer coefficients on pin and endwall surfaces for different staggered arrays of circular pin fins (H/D = 0.5 and 2.0). But the arrays used for the analysis consisted of four rows of pin fins and only channel averaged heat transfer coefficient values were presented. Metzger et al. [5], in 1982 conducted experiments on ten rows of short circular pin fin arrays and studied the heat transfer and pressure drop characteristics. They observed that the Nusselt number increased in the first three to five rows and then gradually decreased through the rest of the array. They also observed that the channel averaged Nusselt numbers were lower compared to the respective long tube array cases for all Reynolds numbers. Metzger et al. [6] studied the pressure drop characteristics for a family of ten row arrays of staggered short circular pin fins and developed friction coefficient correlations which can be applied with good accuracy for a wide range of Reynolds numbers, spacing ratios and height-to-diameter ratios. Armstrong et al. [7] presented a review of staggered circular pin fin array data discussing the effects of pin spacing,

pin height on heat transfer and pressure drop. Existing correlations in the literature for heat transfer and friction factor were presented with a review on their validity and limitation. A short discussion on the areas of pin fin heat transfer and pressure drop that required further research was also presented. Since the trailing edge channel of an airfoil has lateral ejection and flow convergence, efforts were made to study the effects of these parameters. Lateral flow ejection effects on heat transfer and pressure drop were studied for Reynolds numbers between 6,000 and 60,000 by Lau et al. [8]. They concluded that the channel averaged Nusselt number values increased with increasing Reynolds number for any given ejection ratio. They also noticed that as the ejection ratio was increased from 0 to 1, the Nusselt number values reduced for all Reynolds numbers used in the study. Metzger et al. [9] and Hwang et al. [10] conducted experiments by taking into consideration the effect of flow convergence on heat transfer. Some of the recent studies tried to investigate the effect of rotation on heat transfer in rectangular channels with circular pin fins (Willett et al. [11], Wright et al. [12]).

2.   Pin fins of other shapes

Though pin fin shape is an important factor, not many studies have included pin fin arrays of various shapes to analyze the heat transfer and pressure drop characteristics. Metzger et al. [13] considered an array of oblong pin fins and studied the heat transfer and pressure drop characteristics at various attack angles. The heat transfer for oblong pin arrays, which was found to be approximately 20 percent higher compared to the corresponding circular pin arrays was offset by roughly 100 percent increase in pressure drop. Two diamond shaped pin fin geometries were investigated experimentally and numerically by Sparrow and Grannis ([14], [15]) but the focus was on fluid flow and pressure drop characteristics. Tanda [16] performed experiments on

diamond shaped pin fins and studied both the heat transfer and pressure drop trends. Chyu et al. [17] used a mass transfer analogy to study the heat transfer and pressure drop of cubic and diamond pin fins for inline and staggered arrangements. Cubic pin fins were found to produce the highest heat transfer, followed by diamond and circular pin fins and the pressure drop was found to be maximum for diamond pin fins. They suggested cubic pin fins as an alternative to circular pin fins for internal cooling in the trailing edge region of a turbine blade. Numerical studies on inline periodic cubic pin fin arrays were recently conducted by Saha and Acharya [18]. In another experimental work, Goldstein et al. [19] employed naphthalene sublimation technique to study the mass transfer and pressure drop of stepped diameter circular pin fins. The array arrangement was staggered and ten rows of pin fins were used in the streamwise direction. Stepped diameter fins were found to have either higher or same mass transfer as straight cylinder fins but pressure drop was significantly low in the former case. Chen et al. [20] experimentally investigated the heat transfer and pressure drop characteristics of drop shaped pin fin arrays. They noticed that the channel with drop shaped pin fins had higher heat transfer compared to the channel with circular pin fins and the pressure drop of the latter was about double that of the former. The positive results of drop shaped pin fins motivated further research on pin fins with slimmer cross sections. Li et al. [21] experimentally studied short elliptical pin fin arrays in a staggered arrangement. The results of elliptical pin fins were compared with circular pin fins of equal circumference. They noticed that the heat transfer coefficients of elliptical pin fin arrays were higher compared to the corresponding circular pin fin arrays. Also the flow resistance offered by elliptic pin fin arrays was much lower compared to circular pin fin arrays. Uzol and Camci [22] experimentally investigated the heat transfer, pressure drop and flow field measurements downstream in the wake of two row staggered arrays of elliptical and circular

pin fins. Two types of elliptic fins, a SEF fin and an N fin whose minor axis length is same as the diameter of the corresponding circular fin were used for the analysis in order to attain equal effective frontal area. The Nusselt number values for the SEF and N fin arrays were about 27 percent lower on average compared to the circular fin arrays. But the pressure drop values for the SEF and N fin arrays were 59.5 percent and 46.5 percent lower on average compared to the circular fin arrays, respectively. Overall N fins had the highest performance as suggested by the thermal performance indices.

Elliptical pin fins were investigated in the literature and they showed signs of better performance but the work done is not complete. Li et al. [20] presented only the channel averaged values of Nusselt number and Euler number. Uzol and Camci [22] performed the analysis only for two rows of pin fins in the streamwise direction which is not sufficient to set up a fully developed pattern in the test section and the heat transfer, total pressure loss measurements were made downstream of the pin fin rows. An in depth analysis into the flow and heat transfer in rectangular channels with elliptical pin fin arrays is necessary to understand their behavior completely and help improve the design of trailing edges of turbine blades.

3. Research objective

Objective of the current study is to numerically investigate the flow and heat transfer characteristics in a stationary one pass rectangular channel (AR=4:1) with circular and elliptical pin fin arrays. Two types of elliptical pin fins i.e., a SEF and an N fin whose minor axis length is equal to the diameter of the circular fin are used. The analysis is performed with an array of six rows of staggered pin fins in the streamwise direction for Reynolds numbers (Re) of 10,000, 20,000, 30,000, 40,000 and 50,000. 3-D, steady simulations are performed using the low Reynolds number k-omega SST

turbulence model in the FLUENT CFD code.

CHAPTER II

GOVERNING EQUATIONS AND NUMERICAL TECHNIQUE

Turbulent flows are characterized by fluctuating velocity fields. These fluctuations result in the mixing of transported quantities such as momentum, energy and cause the transported quantities to fluctuate as well. Since these fluctuations can be of small scale and high frequency, they are too computationally expensive to simulate directly in practical engineering calculations. Instead, the instantaneous (exact) governing equations can be time-averaged, ensemble-averaged, or otherwise manipulated to remove the small scales, resulting in a modified set of equations that are computationally less expensive to solve. However, the modified equations contain additional unknown variables, and turbulence models are needed to determine these variables in terms of known quantities. It being an extremely complex phenomenon, no single turbulence model approximates the physics of all turbulent flows and is universally accepted as being superior for all classes of problems. The choice of turbulence model depends on considerations such as the physics encompassed in the flow, the established practice for a specific class of problem, the level of accuracy required, the available computational resources, and the amount of time available for the simulation. A number of turbulence models namely zero equation, one equation, two equation and second-moment closure models are available and to make the most appropriate choice of model for an application, understanding the capabilities and limitations of the various options is necessary. Once a turbulence model is selected, an appropriate grid is generated for the domain and the governing equations are solved using a numerical technique to obtain the solution.

For the current study, SST $k - \omega$ two equation turbulence model with a low Reynolds number near wall modeling approach is used. The governing equations are

solved using finite volume method in FLUENT 12.0 CFD code. 3-D structured grid is constructed using the commercial grid generation software GAMBIT 2.3. Grid is generated such that the y^+ of the cell adjacent to wall is less than 1 for the low Reynolds number approach to be valid. The following sections of this chapter concentrate on the governing equations involved, the motive behind the choice of SST $k - \omega$ turbulence model and the numerical procedure used to solve the equations.

A. Governing Equations and Turbulence Model

Time-dependent solutions of the Navier-Stokes equations for high Reynolds-number turbulent flows in complex geometries which set out to resolve all the way down to the smallest scales of the motions are unlikely to be attainable for some time to come. An alternative method can be employed to render the Navier-Stokes equations tractable so that the small-scale turbulent fluctuations do not have to be directly simulated namely Reynolds-averaging (or ensemble-averaging). This method introduces additional terms in the governing equations that need to be modeled in order to achieve a closure for the unknowns.

The Reynolds-averaged Navier-Stokes (RANS) equations govern the transport of the averaged flow quantities, with the whole range of the scales of turbulence being modeled. The RANS-based modeling approach therefore greatly reduces the required computational effort and resources, and is widely adopted for practical engineering applications. The Reynolds averaged continuity and momentum equations for steady, incompressible flow written in Cartesian tensor form are as follows:

$$\frac{\partial \rho}{\partial x_i} + \frac{\partial}{\partial x_i}(\rho u_i) = 0 \tag{2.1}$$

$$\frac{\partial}{\partial x_j}(\rho u_i u_j) = -\frac{\partial p}{\partial x_i} + \frac{\partial}{\partial x_j}\left[\mu(\frac{\partial u_i}{\partial x_j} + \frac{\partial u_j}{\partial x_i} - \frac{2}{3}\delta_{ij}\frac{\partial u_i}{\partial x_i})\right] + \frac{\partial}{\partial x_j}(-\rho \overline{u'_i u'_j}) \tag{2.2}$$

The flow is assumed to be incompressible because of the very low Mach number but the density change due to the differences in temperature is taken into consideration using $\rho = \rho_0 T_0 / T$. Reynolds analogy, which relates the turbulent momentum to heat transfer is used to model the turbulent heat transfer. The resulting energy equation is as follows:

$$\frac{\partial}{\partial x_i}[u_i(\rho E + p)] = \frac{\partial}{\partial x_i}\left[(k + k_t)\frac{\partial T}{\partial x_i} + u_j(\tau_{ij})_{eff}\right] \tag{2.3}$$

where k_t is the turbulent thermal conductivity and $(\tau_{ij})_{eff}$ is the deviatoric stress tensor. The first and the second term on the right hand side of Eq. 2.3 represent energy transfer due to conduction and viscous dissipation, respectively.

Eq. 2.1 and 2.2 have the same general form as the instantaneous Navier-Stokes equations, with the velocities and other solution variables now representing ensemble-averaged (or time-averaged) values. Additional terms are introduced now which represent the effects of turbulence. These additional terms, $-\rho\overline{u_i' u_j'}$ (Reynolds stresses), must be modeled in order to close Eq. 2.2. A common method employs the Boussinesq hypothesis to relate the Reynolds stresses to the mean velocity gradients:

$$-\rho\overline{u_i' u_j'} = \mu_t\left(\frac{\partial u_i}{\partial x_j} + \frac{\partial u_j}{\partial x_i}\right) - \frac{2}{3}\left(\rho k + \mu_t\frac{\partial u_k}{\partial x_k}\right) \tag{2.4}$$

The Boussinesq hypothesis is used in the $k - \epsilon$ models, and the $k - \omega$ models. The advantage of this approach is the relatively low computational cost associated with the computation of the turbulent viscosity, μ_t. In the case of the $k - \epsilon$ and $k - \omega$ models, two additional transport equations (for the turbulence kinetic energy, k, and either the turbulence dissipation rate, ϵ, or the specific dissipation rate, ω) are solved, and μ_t is computed as a function of k and either ϵ or ω.

The $k - \epsilon$ model is the most popular two equation model and has been shown to be useful for flows with relatively small pressure gradients. But the model gives accurate

results only in problems where average pressure gradients are small. Reduction in accuracy was observed for flows containing large adverse pressure gradients and flow separation. Owing to the large separation and reattachment involved in a pin fin array problem, $k - \epsilon$ model is not recommended for the current study. The $k - \omega$ model which is an alternative to the $k - \epsilon$ model has shown improved performance for flows with moderate adverse pressure gradients. Another significant advantage of $k - \omega$ model is that it may be applied throughout the boundary layer, including the viscous-dominated region, without further modification. In its original form, $k - \omega$ model suffers a major drawback which is the high sensitivity of the ω equation to the values of ω in the free stream which inturn modifies into extreme sensitivity to inlet boundary conditions for internal flows, a problem that does not exist for the $k - \epsilon$ model. This hindered the $k - \omega$ model from being applied to practical flow simulations over $k - \epsilon$ model. The problem of sensitivity to free-stream/inlet conditions is addressed in the SST $k - \omega$ model which effectively blends the accurate and robust formulation of the $k - \omega$ model in the near wall region with the free stream independence of the $k - \epsilon$ model in the far field. This is achieved by transforming the ϵ transport equation into an ω transport equation by variable substitution. The SST $k - \omega$ model and standard $k - \omega$ model are similar to each other except for a few refinements. The standard model $k - \omega$ model and the transformed $k - \epsilon$ model are both multiplied by a blending function and both models are added together. The blending function is designed to be one in the near wall region, which activates the standard $k - \omega$ model, and zero away from the surface, which activates the transformed $k - \epsilon$ model. The SST model incorporates a damped cross diffusion derivative term in the ω equation and the definition of the turbulent viscosity is modified to account for the transport of the turbulent shear stress. Because of these features, the SST $k - \omega$ model can be applied to a wider class of flows (e.g., adverse pressure gradient

flows, airfoils) with great accuracy and reliability. Transport equations for the SST $k - \omega$ model are as follows:

$$\frac{\partial}{\partial x_i}(\rho k u_i) = \frac{\partial}{\partial x_j}\left(\Gamma_k \frac{\partial k}{\partial x_j}\right) + G_k - Y_k \tag{2.5}$$

$$\frac{\partial}{\partial x_i}(\rho \omega u_i) = \frac{\partial}{\partial x_j}\left(\Gamma_\omega \frac{\partial \omega}{\partial x_j}\right) + G_\omega - Y_\omega \tag{2.6}$$

In these equations, G_k represents the generation of k due to mean velocity gradients and G_ω represents the generation of ω. Γ_k and Γ_ω represent the effective diffusivity of k and ω, respectively. Y_k and Y_ω represent the dissipation of k and ω due to turbulence. More information on the calculation of all the above terms can be found in FLUENT documentation [23].

B. Near Wall Modeling

In the presence of a no-slip wall, turbulent flows are significantly affected because of the large gradients in solution variables. Effects of viscosity on the transport processes are also large. The technique used to model the near wall region significantly affects the accuracy of the numerical solution. Therefore, accurate representation of the flow in the near wall region is essential for successful prediction of wall bounded turbulent flows.

The near wall region can be subdivided into three layers. The innermost layer is known as "viscous sublayer". The flow is almost laminar in this region with the transport processes being dominated by (molecular) viscosity. The outer layer is called as "fully turbulent layer" and turbulence dominates the transport process in this region. Finally there is an intermediate region called the "buffer layer" between viscous sublayer and fully turbulent layer where both molecular viscosity and turbulence play a vital role in the transport process.

The flow in the near wall region is typically modeled using the following two approaches.

- The first approach employs "wall functions" which are semi-empirical formulae used to connect the no-slip wall and the fully turbulent region through the viscosity affected region which actually resolving it.

- The second approach employs "low Reynolds number" method in which the turbulence models are modified so that even the near wall region can be resolved with a mesh all the way down to the wall.

The important advantage of wall function approach is the drastic reduction in the usage of computational resources with reasonably accurate solutions. The wall function approach is popularly used in industrial flow simulations. All high Reynolds number models can be used with this approach. On the other hand, when the low Reynolds number effects are dominant and solution variables in the near wall region are important for the study, low Reynolds approach is recommended. Despite the heavy computational resources taken by this approach because of the refined mesh in the near wall region, the solution accuracy is higher compared to wall function approach. SST or Wilcox models which are based on the ω equation can be used with this low Reynolds number approach. Local velocity profiles and heat transfer augmentation details are important for the current study which makes the low Reynolds number approach, the obvious choice for near wall modeling. More information on the low Reynolds approach and the mesh requirements for it to be valid can be found in FLUENT documentation [23].

C.   Numerical Technique

The next step after deciding the governing equations and generating the grid is to solve them numerically. FLUENT employs a control volume technique wherein the scalar governing equation is converted into a discretized equation by integrating it about each control volume. The discretized equations are then linearized and the resulting linear system of equations are solved to obtain the updated values of variables. FLUENT offers two solvers namely pressure based solver and density based solver. Both models can be used for a wide range of flows but the pressure based solver has historically been used for incompressible flows. Pressure based solver further offers two algorithms: a segregated algorithm, and a coupled algorithm. The individual governing equations are solved sequentially in a segregated algorithm and simultaneously in a coupled algorithm. So the memory requirements for coupled algorithm are considerably higher compared to segregated algorithm. Because of the above reasons, pressure based segregated algorithm is used to solve flow, energy and turbulence equations. Second order upwind scheme is used to spatially discretize the momentum, energy, turbulence kinetic energy and specific dissipation rate equations. For pressure interpolation and pressure-velocity coupling, STANDARD scheme and SIMPLE scheme are used respectively. Gradients and derivatives are evaluated using Green-Gauss Cell Based technique. A convergence criterion of 10^{-3} is used for continuity equation, 10^{-4} for momentum, turbulence kinetic energy and specific dissipation rate equations and 10^{-7} for energy equation. In addition, area weighted averages of velocity magnitude and heat flux are monitored on the outlet and bottom wall respectively.

CHAPTER III

FLOW AND HEAT TRANSFER IN A SINGLE PASS RECTANGULAR
CHANNEL WITH PIN FINS

Computations are performed in this chapter for a stationary one pass rectangular channel (AR=4:1) as tested by Wright et al. [12] for circular and elliptical pin fins using the low Reynolds number k-omega SST turbulence model in FLUENT.

A.   Pin Fin Shapes

Three different pin fin shapes (one circular and two elliptical) are investigated in the current study. The two elliptical pin fins used are Standard Elliptical Fin (SEF) and N fin. Fig. 2 depicts the shapes and the relative dimensions of the three pin fins. The minor axis lengths of both SEF and N fin are kept equal to the diameter
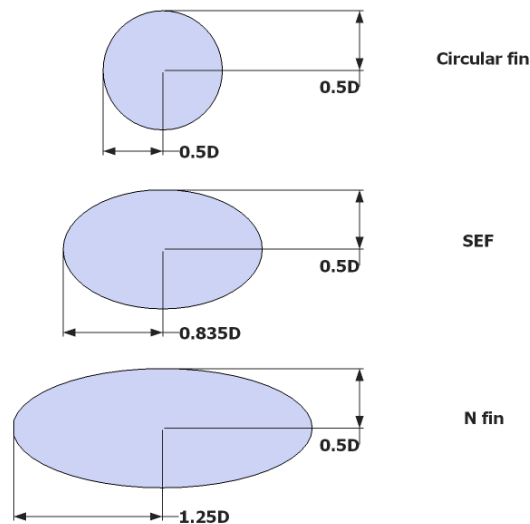

Fig. 2. Pin fin shapes and their relative dimensions

of the circular fin which results in same effective frontal area. More information on the description of SEF and N fin can be found in Uzol and Camci [22] who used the same pin fin shapes for their comparison studies.

B. Description of the Problem

The test section and the pin fin configuration used in the current study are illustrated in Fig. 3. Because of the symmetry of flow with respect to y and z directions, the flow is simulated only for one quarter of the channel. The test section of Fig. 3 for circular fins is identical to Wright et al. [12] except for the number of rows of pin fins used in the streamwise direction. Due to the non-availability of computational resources, simulations are performed only for six rows of pin fins instead of the twelve rows as in Wright et al. [12]. Fig. 3 depicts the pin fin configuration for circular pin fins. The constraints used while installing the SEF and N fins are that the leading edges of both the pin fin shapes are placed such that they share the exact same location as that of the leading edge of circular pin fin and also that the major and minor axes are parallel to streamwise and spanwise direction respectively.

The test section is a one pass rectangular channel with a channel aspect ratio (AR) of 4:1. It starts with an unheated smooth section (L_1/D_h=1.0) followed by a heated section (L_2/D_h=4.384) with pin fins and ends with an unheated smooth section (L_3/D_h=4.877). The two walls of heated section perpendicular to y direction are designated as side walls and the two walls perpendicular to z direction are designated as bottom and top walls. The hydraulic diameter (D_h) of the channel is 0.0203 m.
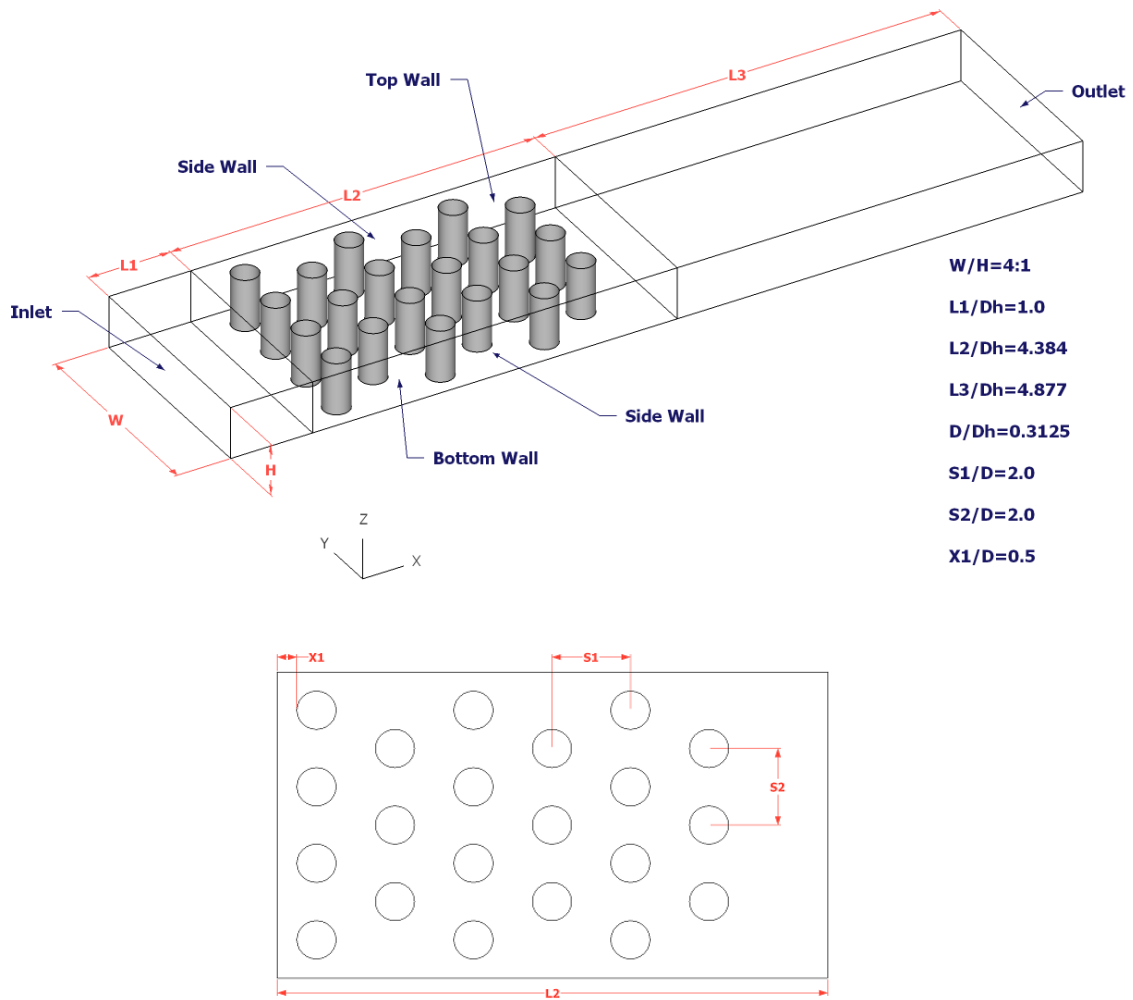
Fig. 3. Schematic of the test section with pin fins

1. Boundary conditions

Fully developed flow conditions are used at the inlet of the test section. 3-D simulations are performed separately on a smooth unheated rectangular channel whose cross sectional dimensions are same as that of the test section for all Reynolds numbers studied in the current work. Uniform flow conditions are used at the inlet of this rectangular channel and using a sufficient length for the channel, fully developed flow conditions are obtained at the outlet. The outlet flow conditions are then ex-

ported and used as the inlet conditions for the test section. Computational time can be minimized drastically by using this procedure for obtaining fully developed flow. Outflow boundary condition is used at the outlet of the test section because of no prior information regarding the conditions at the outlet. Air which is used as the coolant enters the inlet of the test section at uniform temperature $(T = T_o)$. Zero flux boundary condition is used on the walls of unheated sections and a constant temperature condition $(T = T_w)$is used on all the walls (side walls, bottom wall, top wall, pin fin walls) of heated section. The Reynolds numbers (Re) studied in the current work are 10,000, 20,000, 30,000, 40,000, 50,000 and the inlet coolant-to-wall density ratio $(\Delta\rho/\rho)$ is maintained at 0.122. Since the flow is being simulated for one quarter of the channel, symmetry boundary conditions are used on the planes of symmetry in both y and z directions.

C. Grid Details and Independence

Commercial grid generation software GAMBIT 2.3 is used to build the model and mesh it using a structured hexagonal mesh. For grid independence study, simulations are performed on one quarter of the test section of Fig. 3 but two instead of six rows of fins are used in the heated section to reduce computational time and the spanwise Nusselt number ratio plots are compared for three different grid resolutions. Fig. 4

Table I. Details of the grid used for the test section with six rows of pin fins

	Channel	Pin fin	Total
Circular fin	390 x 90 x 40	90 x 28 x 40	2,278,600
SEF	434 x 80 x 40	100 x 27 x 40	2,174,960
N fin	440 x 82 x 39	120 x 24 x 39	2,195,856

show that the spanwise Nusselt number ratio values (presented only upto $X/D_h = 2.5$) for the grid with highest resolution do not vary much when compared to the other grid resolutions and can be considered grid independent. So the number of grid points used for the most refined mesh are carried forward to the test section with six rows of fins. Fig. 5 shows the grid used for the heated section of the channel for all the fin shapes and Table I lists the number of grid points used. The minimum grid spacing for all Reynolds numbers is maintained at 10^{-4} of the hydraulic diameter which results in wall y^+ values of less than 1.
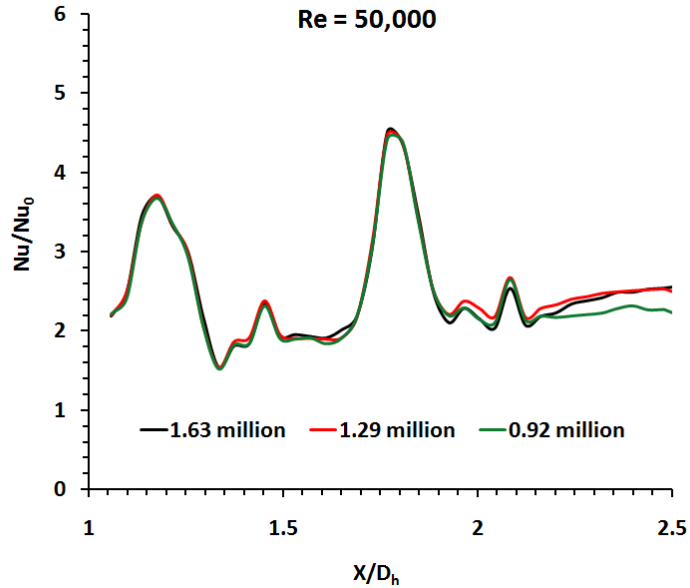

Fig. 4. Grid independence study for circular pin fins

D. Validation Study

As mentioned previously in section B of Chapter III, the current test section for circular fins is identical to Wright et al. [12] except that the number of rows of pin fins used in the streamwise direction are six instead of twelve. This is a reasonable
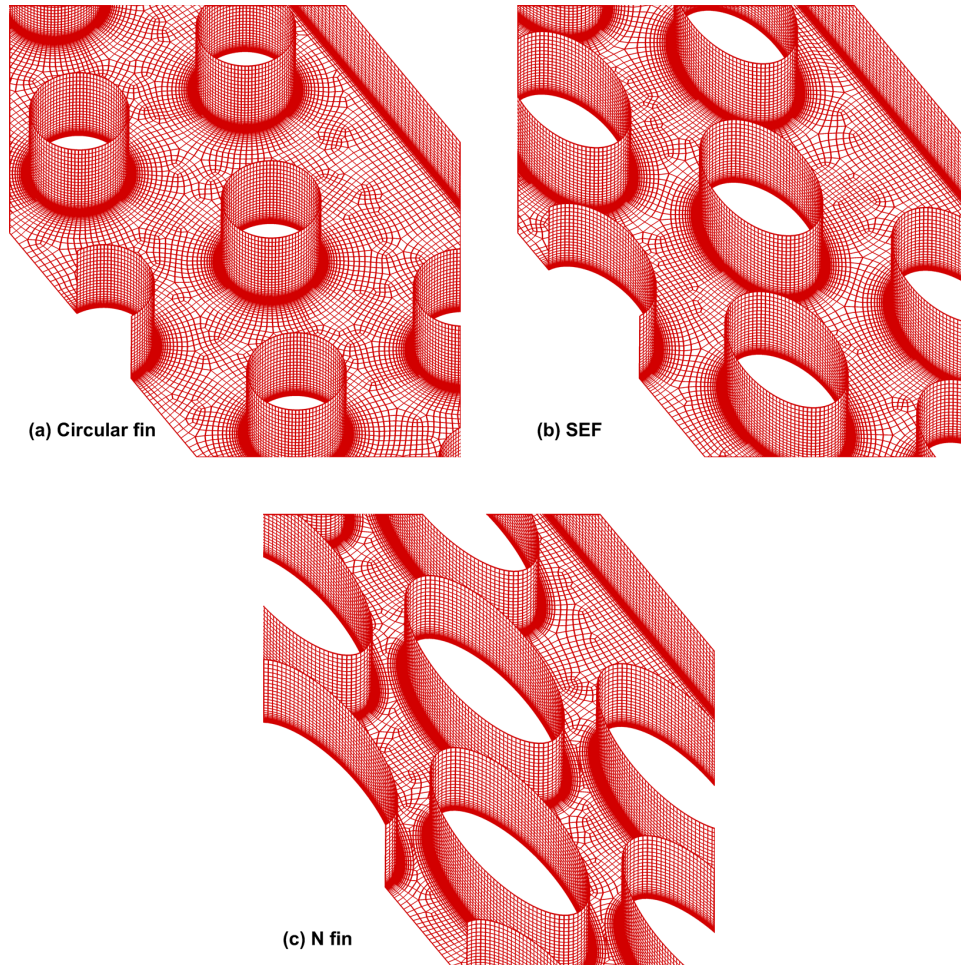
Fig. 5. Computational grid used for the heated section

simplification since Wright et al. [12] data shows very little change after the sixth row for non-rotating cases and can be considered periodic. So the heat transfer data of the current study for circular fins are validated using Wright et al. [12]. The Nusselt number values are normalized using the Dittus-Boelter correlation for a smooth tube which is as follows:

$$Nu_0 = 0.023 Re^{0.8} Pr^{0.4} \tag{3.1}$$

Fig. 6 shows the spanwise averaged and regional averaged (spanwise average over every two rows of pin fins) values of Nusselt number ratio (Nu/Nu_0) plotted against
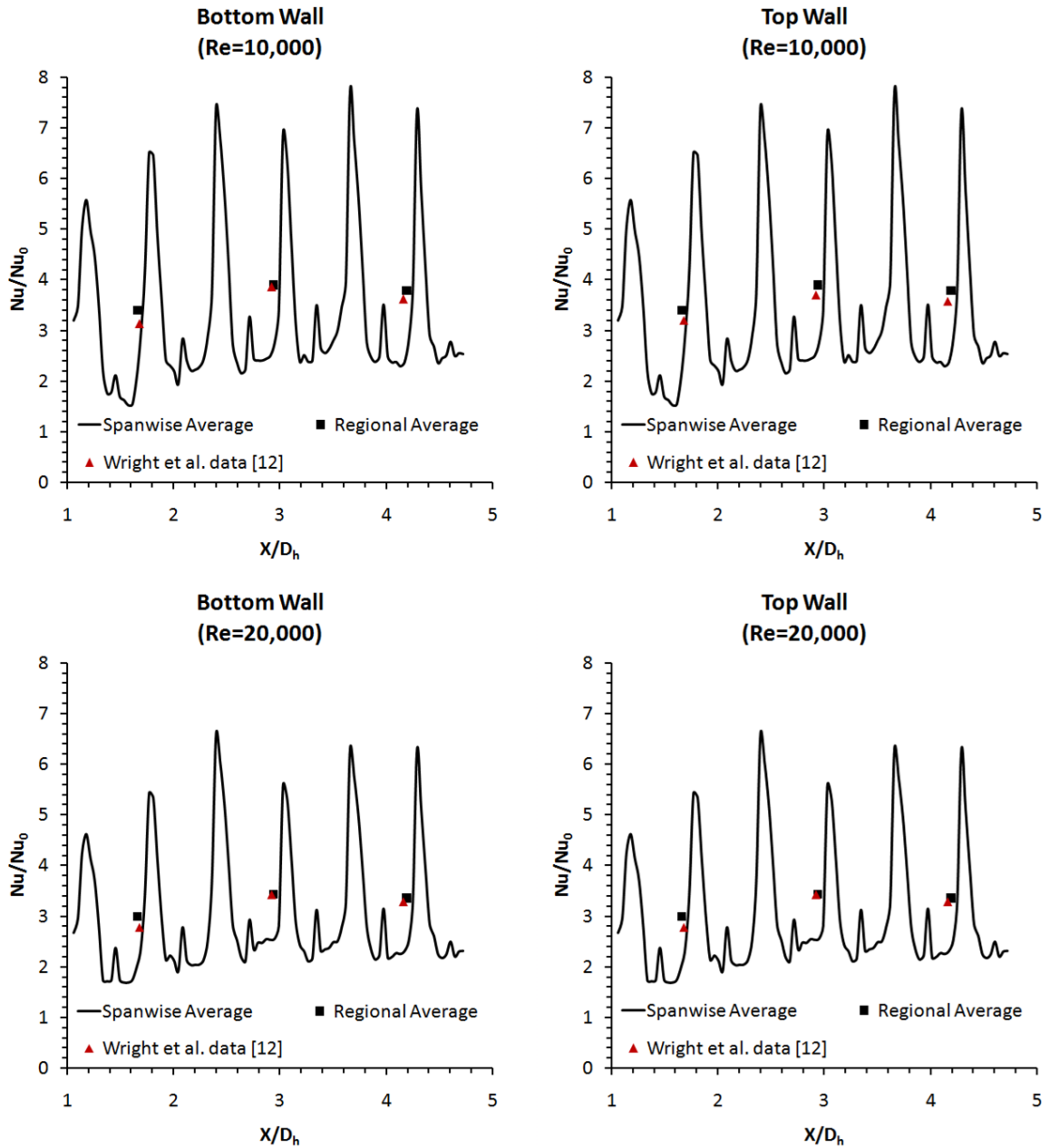
Fig. 6. Comparison between current numerical data and published experimental data of regional averaged Nusselt number ratio values for circular fin array

Reynolds number (Re). The expressions of Nusselt number (Nu) and Reynolds number (Re) used in the current study are as follows:

$$\text{Nu} = \frac{hD_h}{k} \tag{3.2}$$

$$\text{Re} = \frac{\rho V_m D_h}{\mu} \tag{3.3}$$

Good agreement between the regional averaged values of Nusselt number ratio (Nu/Nu_0) and Wright et al. [12] data support the ability of the current numerical model to accurately predict the heat transfer data for channels with circular pin fins. Due to the non-availability of pressure data in Wright et al. [12], the friction coefficient values are validated using the correlations developed experimentally by Metzger et al. [6] which can be applied for a wide range of spacing, pin-height to diameter ratios. The friction coefficient (f^*) and Reynolds number (Re_D) expressions as defined in Metzger et al. [6] are as follows:

$$f^* = \frac{\Delta P}{2\rho V_{max}^2 N} \tag{3.4}$$

$$\text{Re}_D = \frac{\rho V_{max} D}{\mu} \tag{3.5}$$

where ΔP denotes pressure drop, ρ denotes density of fluid, V_{max} denotes mean velocity at minimum flow area, and N denotes number of rows of pin fins. Fig. 7 shows that the numerical friction coefficient data match closely with the experiments for all Reynolds numbers investigated in the current study. The maximum deviation from the experiments is 14.3% which falls under the $\pm 15\%$ error bar as proposed by Metzger et al. [6].

Apart from the above validation, it is also necessary to test the ability of the current model to accurately predict data for SEF and N fin geometries. So the experiments performed by Uzol and Camci [22] on SEF and N fins are emulated and the numerical data are compared with experiments for Reynolds numbers (Re_D) 20,199,
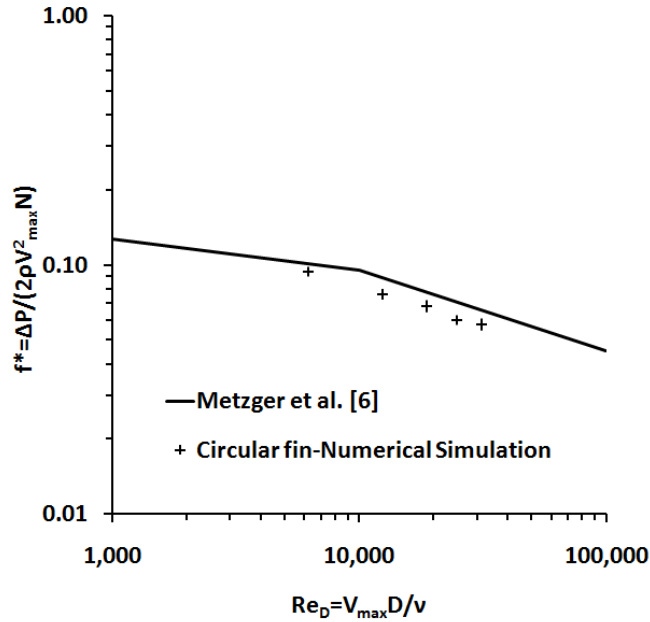
Fig. 7. Comparison between current numerical data and published experimental data
of friction coefficient (f^*) values for circular fin array

26,932 and 33,665. Building and meshing of model, grid independence are done sep-
arately for this validation study. Fig. 8 presents the line averaged Nusselt number
(Nu_D) and friction coefficient (f^{**}) data which clearly depicts a good agreement be-
tween simulation and experimental results. Fig. 9 is a contour plot of velocity on
the midplane of symmetry for $\mathrm{Re}_D = 20{,}199$. The size of the wake for N fin array is
very less in comparison to SEF array which explains the reason behind lower friction
coefficient values in Fig. 9 for the former. The definitions of Nusselt number (Nu_D)
and friction coefficient (f^{**}) used by Uzol and Camci [22] are as follows:

$$\mathrm{Nu}_D = \frac{hD}{k} \qquad (3.6)$$

$$f^{**} = \frac{P_{t_i} - P_{t_w}}{0.5\rho V_{max}^2 N} \tag{3.7}$$

where P_{t_i} indicates total pressure at the inlet of test section and P_{t_w} indicates total

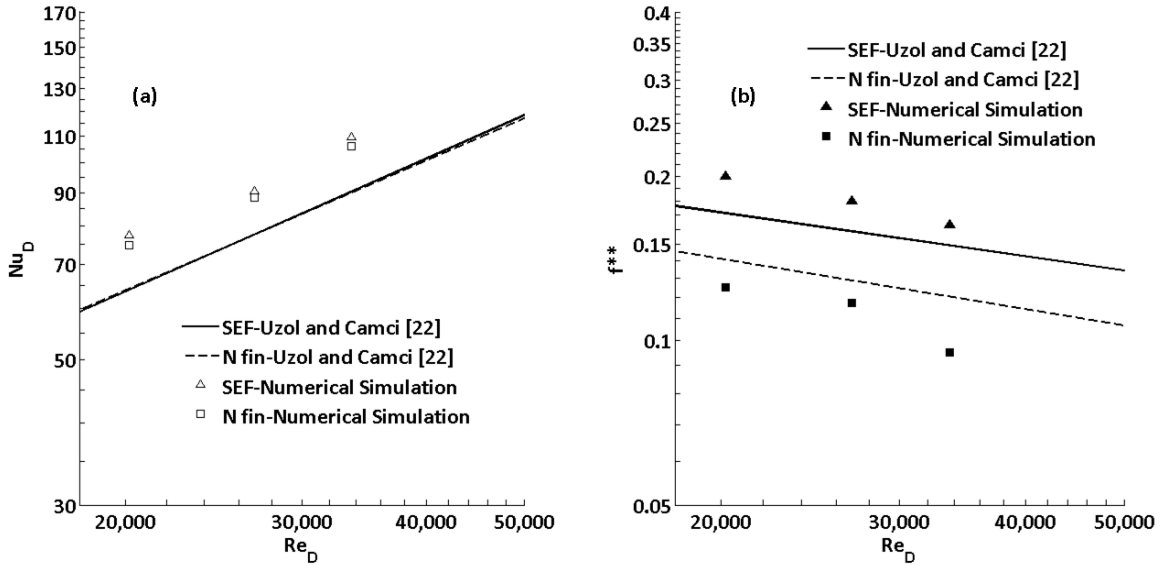pressure $2D$ downstream of the pin fin arrays.

Fig. 8. Comparison between current numerical data and published experimental data
(Uzol and Camci [22]) for SEF and N fin shapes (a) Nusselt number (Nu_D) (b)
friction coefficient (f^{**})

E.   Velocity Field

In the current study, minor axis lengths of both SEF and N fin are kept equal to

the diameter of the circular fin which results in same effective frontal area and helps

in making coherent velocity field and friction factor comparisons. Fig. 10 presents

the vector plot of velocity on the midplane of symmetry for Re = 10,000. Typical

of flow through pin fin array, the mainstream flow impinges on the first row of pin

fins, accelerates around it and then boundary layer separation occurs which results
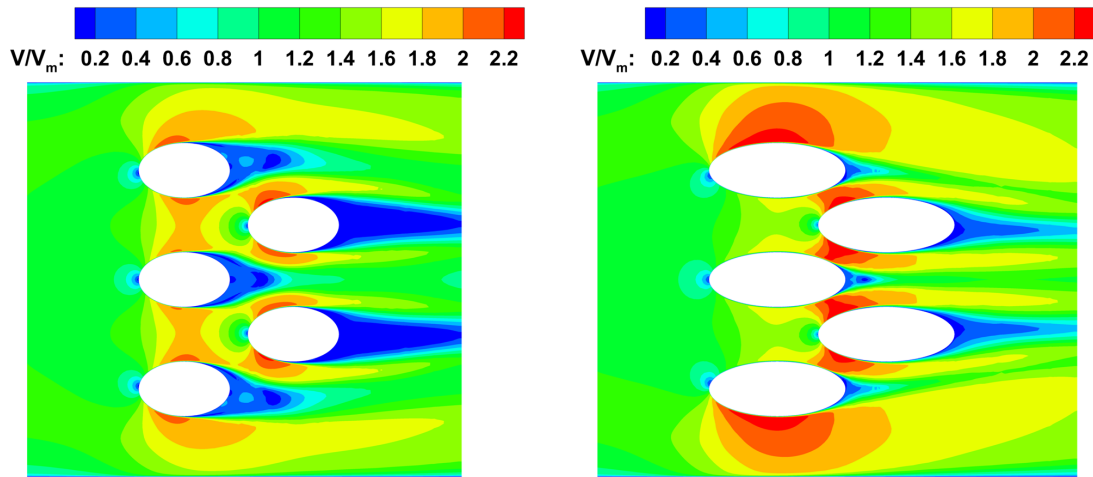
Fig. 9. Contours of velocity on midplane of symmetry for $\mathrm{Re}_D = 20,199$ (validation study)

in wakes downstream of the pin fin row. Due to the staggered arrangement, the impingement on the second row is mostly due to the mainstream flow. Once again the flow accelerates, boundary layer separation occurs which results in wakes downstream of the second row. The flow mixes as it passes through the first two rows of pin fins, gets sufficiently mixed by the third row and follows a roughly periodic pattern in the subsequent rows. The heat transfer is enhanced due to the increase in turbulence because of the acceleration of the flow around pin fins, due to the impingement of accelerated flow on the leading edge of pin fins and also due to the constant breaking of the boundary layer on the bottom wall. Figs. 11, 12, 13 show a zoomed in view of the vector plot for the third and the fourth pin fin row. It can be observed that the size of the wake reduces as the major axis length increases for constant Reynolds number and also as the Reynolds number increases for constant major axis length.
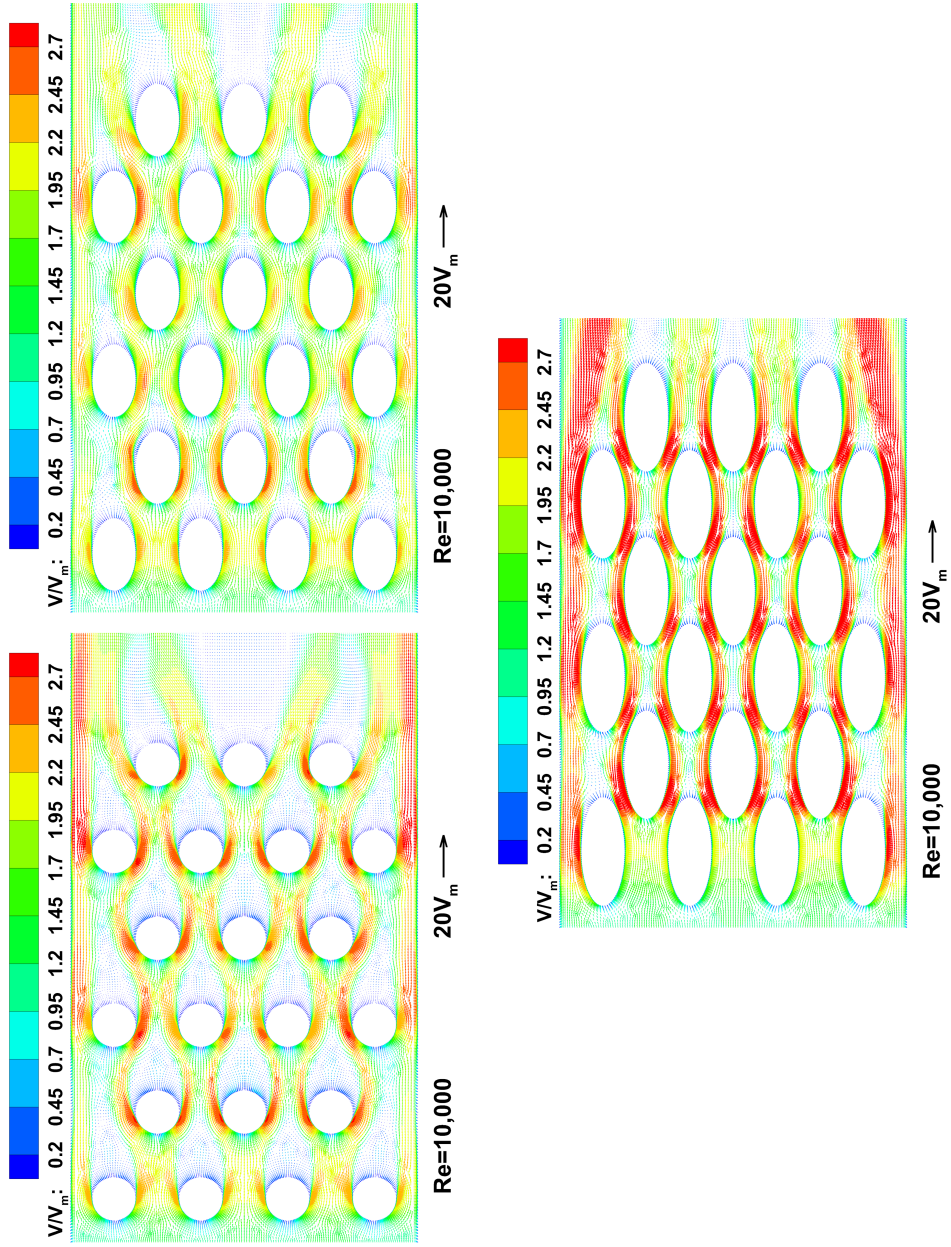
Fig. 10. Velocity vectors on midplane of symmetry showing six rows of pin fins

Another very important deduction from Figs. 11, 12, 13 is that as the major axis length increases, the interaction between consecutive pin fin rows also increases as the spacing ratio is constant. Now the "size of the wake" and the "interaction between consecutive rows of pin fins" have similar effect on heat transfer and pressure loss. As the size of the wake increases, the deceleration of the flow downstream of pin fins decreases which results in higher pressure loss and heat transfer. As the interaction between consecutive rows of pin fins increases, the acceleration of flow in the gaps (between consecutive pin fin rows) increases which results in higher pressure loss and heat transfer. The effective result of these two parameters on pressure loss and heat transfer for the three pin fin shapes will be discussed in the following sections. Finally it is important to note that the wakes of pin fins closest to the side wall in odd numbered rows in circular fin and SEF arrays are skewed towards the side wall but relatively straight in N fin array which indicates the higher interaction between pin fins and side wall in N fin array.

F.   Pressure Loss

Pressure loss in a smooth channel is exclusively due to skin friction which is caused by the friction between wall and fluid. It is a completely different story in a channel with pin fins where the pressure loss is a combination of skin friction and form drag with the latter playing a dominant role. As the flow passes over pin fins, boundary layer separates and wakes are formed downstream of the pin fins. This creates a high pressure region near leading edge and low pressure region near trailing edge of pin fins. The pressure loss caused due to this phenomenon is termed as form drag which increases as the number of pin fins increase. This is the reason behind higher friction coefficient value for a pin fin channel when compared to a smooth
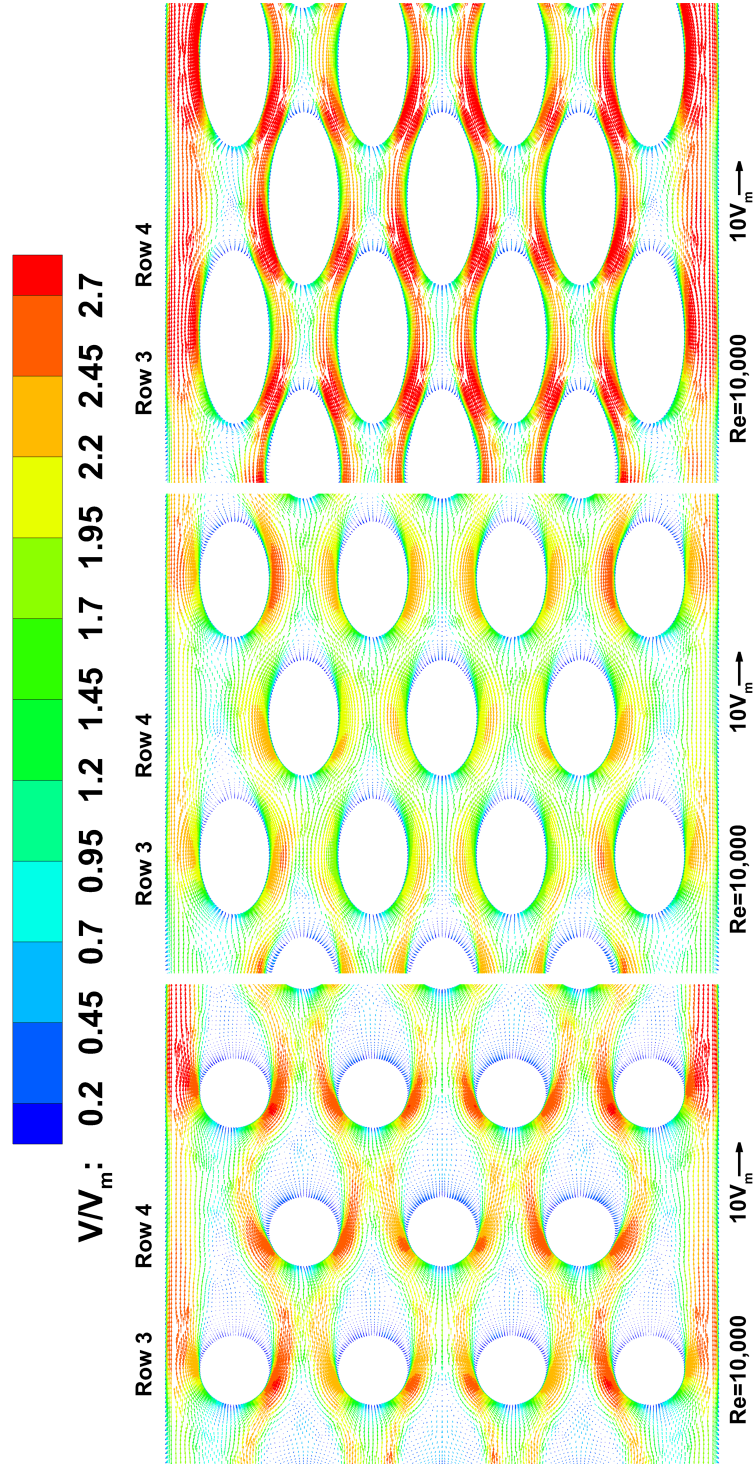
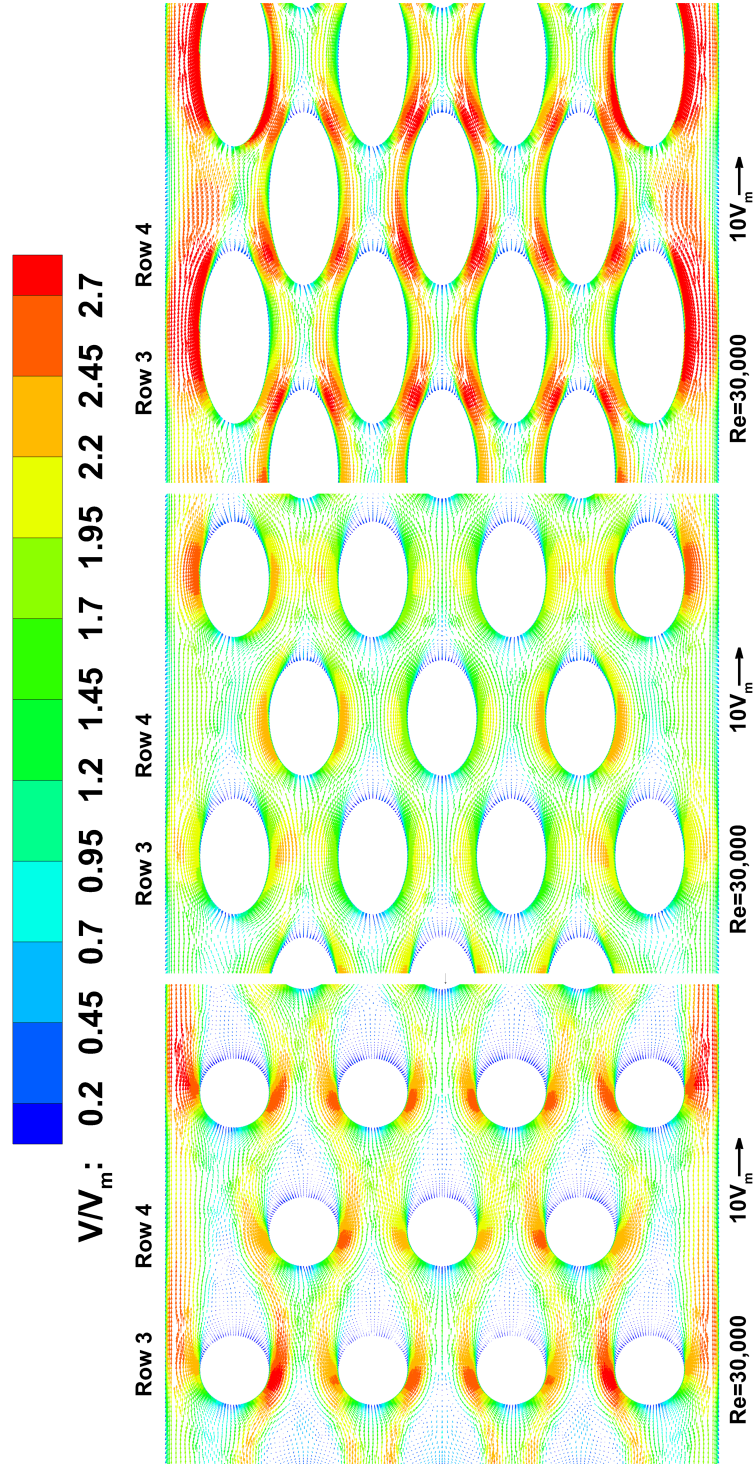Fig. 11. Closer view of velocity vectors on midplane of symmetry (Re=10,000)

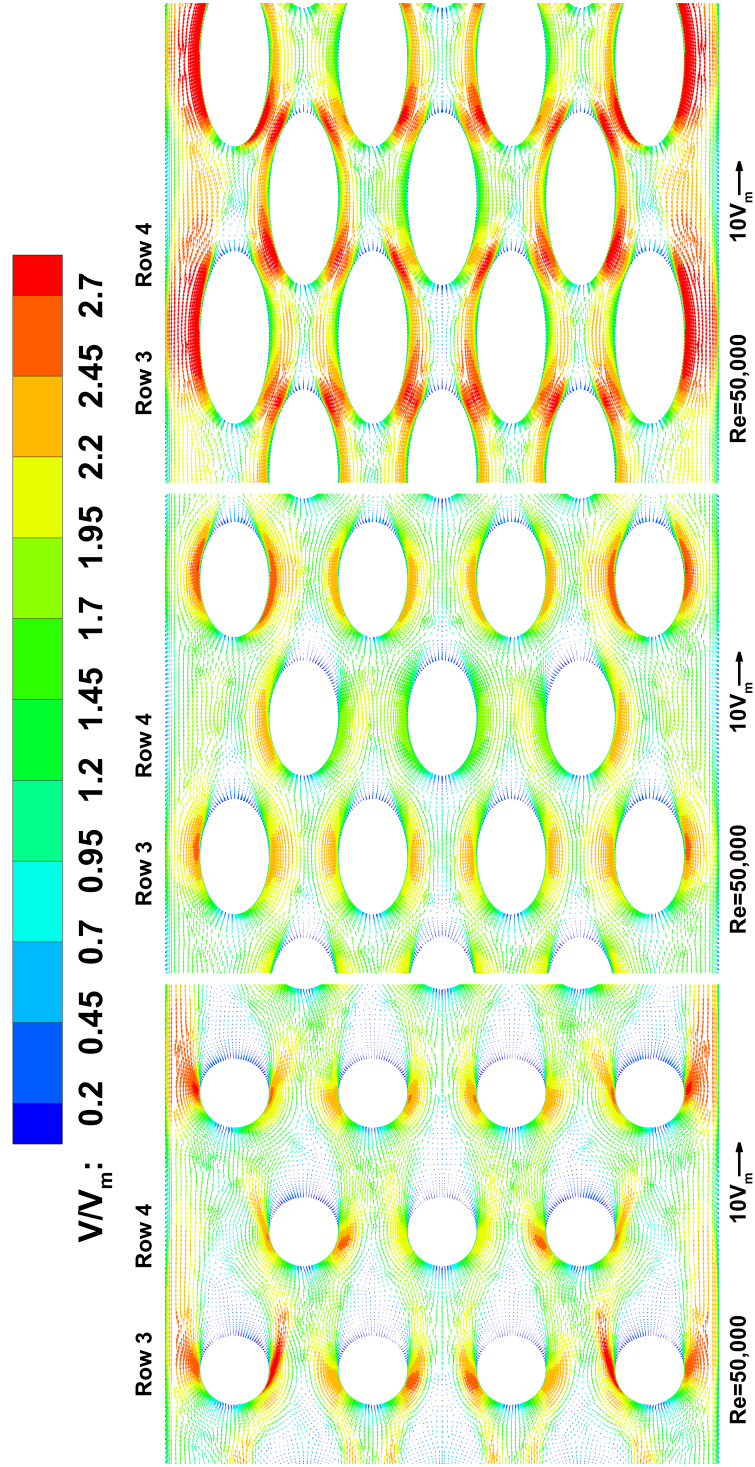Fig. 12. Closer view of velocity vectors on midplane of symmetry (Re=30,000)

Fig. 13. Closer view of velocity vectors on midplane of symmetry (Re=50,000)

channel. Fig. 14 presents the variation of friction coefficient (f) values with Re for all fin shapes. The friction coefficient (f) used in the present study is defined as follows:

$$f = \frac{D_h}{2\rho V_m^2} \left| \frac{dP}{dx} \right| \tag{3.8}$$

where dP/dx, which is the pressure gradient is obtained by calculating area weighted average of pressure at numerous cross sections along the streamwise direction from the inlet of heated section to $0.5D$ downstream of the trailing edge of last pin fin row, plotting these pressure values on a graph against the streamwise direction and evaluating the slope of the best fitted line through the points.
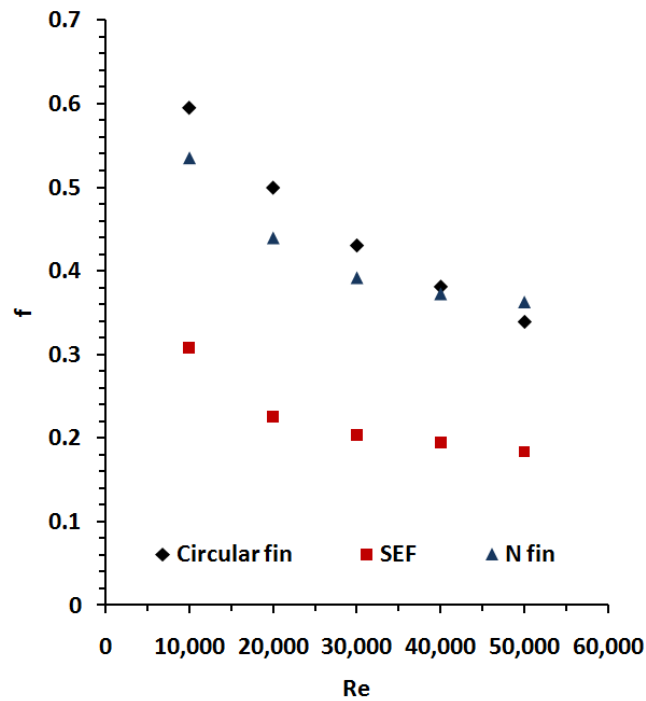

Fig. 14. Friction coefficient versus Reynolds number for circular, SEF and N fin arrays

The friction coefficient values in Fig. 14 decrease with increase in Re for constant major axis length. This is probably because the size of wakes in Figs. 11, 12, 13 go
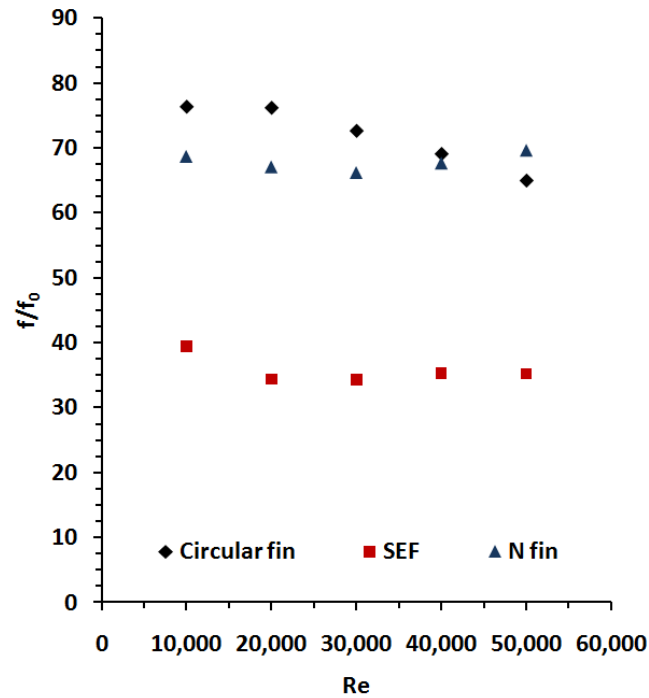
Fig. 15. Friction coefficient ratio versus Reynolds number for circular, SEF and N fin arrays

down as Reynolds number increases for all fin shapes which results in lower form drag. Also circular and N fin arrays have similar f values which are significantly higher than the values exhibited by SEF array. As discussed in section E of Chapter III, the "size of the wake" is largest in circular fin array and least in N fin array whereas the "interaction between consecutive rows of pin fins" is highest in N fin array and lowest in circular fin array for a fixed Re which is possibly the reason behind their similar f values. But in the case of SEF array, the placement of the fins is such that both parameters are not too high which probably explains why they have lower f values. Another important observation from Fig. 14 is that for Re = 10,000, circular fin array has slightly higher f value when compared to N fin array and as the Reynolds number

increases, the gap closes down and eventually the f value of N fin array becomes more than that of circular fin array for Re = 50,000. This is probably because of the fact that "size of the wake" reduces but "interaction between consecutive rows of pin fins" remains constant with increasing Re for a fixed shape. Finally the friction coefficient ratio (f/f_0) values are plotted against Reynolds number in Fig. 15 where the Blasius equation $(f_0 = 0.078\text{Re}^{-0.25})$ is used to normalize the f values. It is evident that the f/f_0 values are almost independent of Re for SEF and N fin arrays and slightly dependant on Re for circular fin array.

G.   Heat Transfer

Figs. 16, 17, 18 present the contour plots of Nu/Nu_0 on bottom wall, pin wall separately (pin fin contours are provided for half their length for clear view) and Fig. 19 presents the spanwise averaged values of Nu/Nu_0 on bottom wall, pin wall combined together. It is evident that the highest Nu/Nu_0 values are achieved near the location of leading edge of pin fins because of the impingement of high velocity flow and lowest Nu/Nu_0 values are obtained near the trailing edge region of pin fins because of the presence of wakes. Also the Nu/Nu_0 values increase in the first three rows and roughly periodic behaviour is shown by alternate rows subsequently. This is because of the fact that the flow impinging on the first two rows is mostly the mainstream flow, not sufficiently mixed and at a lower velocity unlike the flow impinging on the later rows which is sufficiently mixed (hence the roughly periodic behavior) and at a higher velocity. The difference in maximum Nu/Nu_0 values between odd and even numbered rows is because of the higher interaction between pin fins and side wall in the former leading to a higher maximum Nu/Nu_0 value. Another notable observation is that with increasing Reynolds number, Nu/Nu_0 values on the bottom wall and the
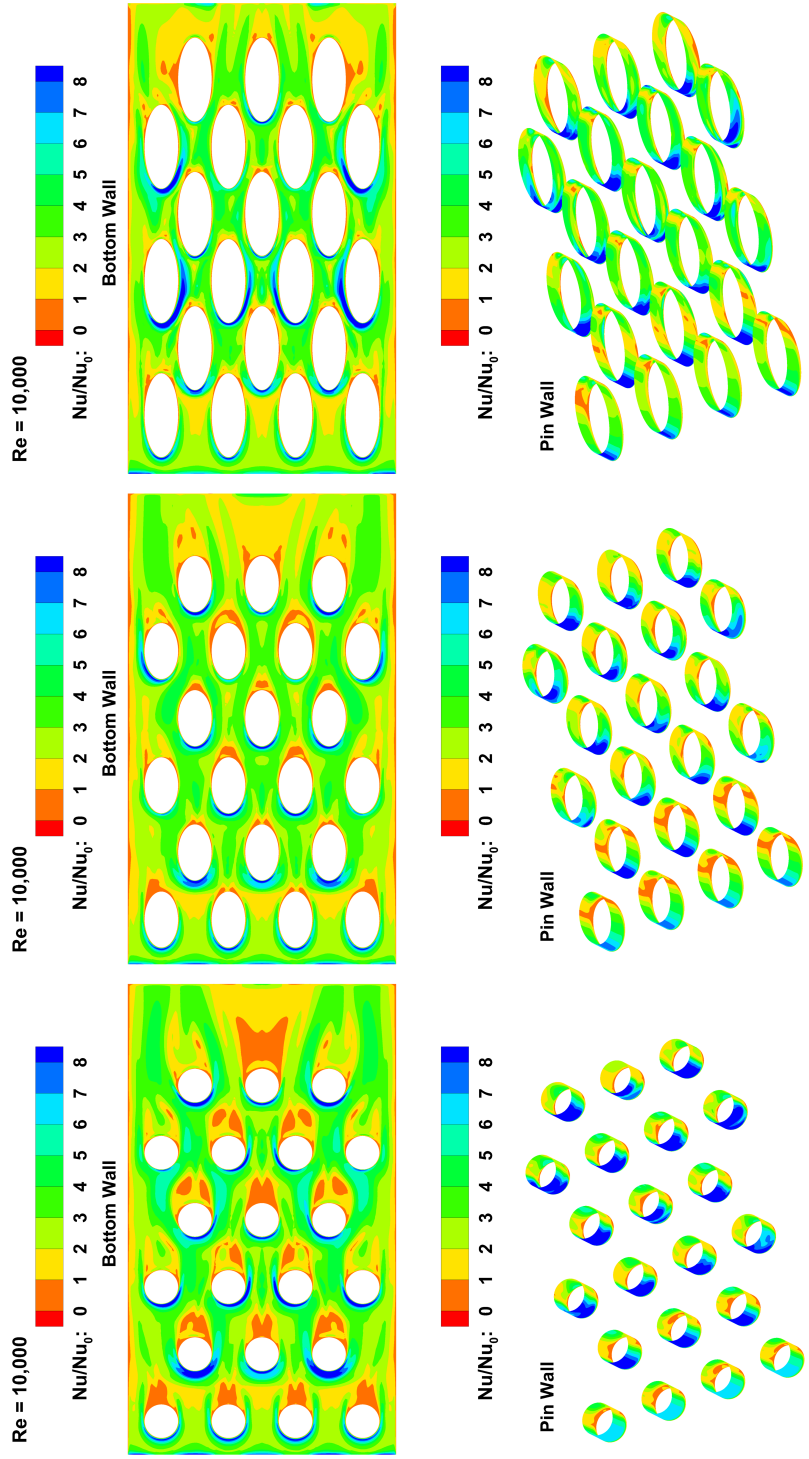
Fig. 16. Contours of Nusselt number ratio on bottom wall and pin wall for circular, SEF and N fin arrays (Re=10,000)
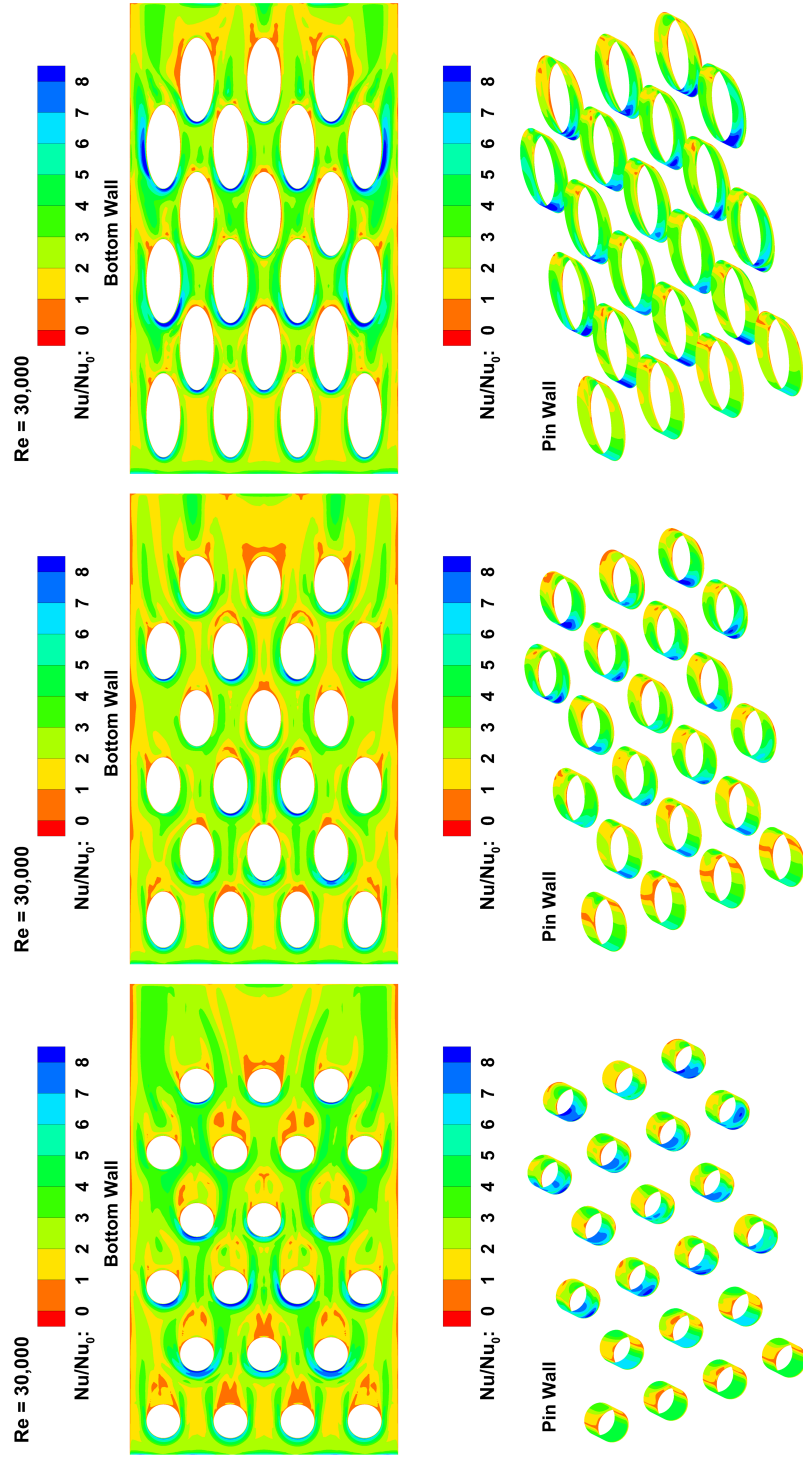
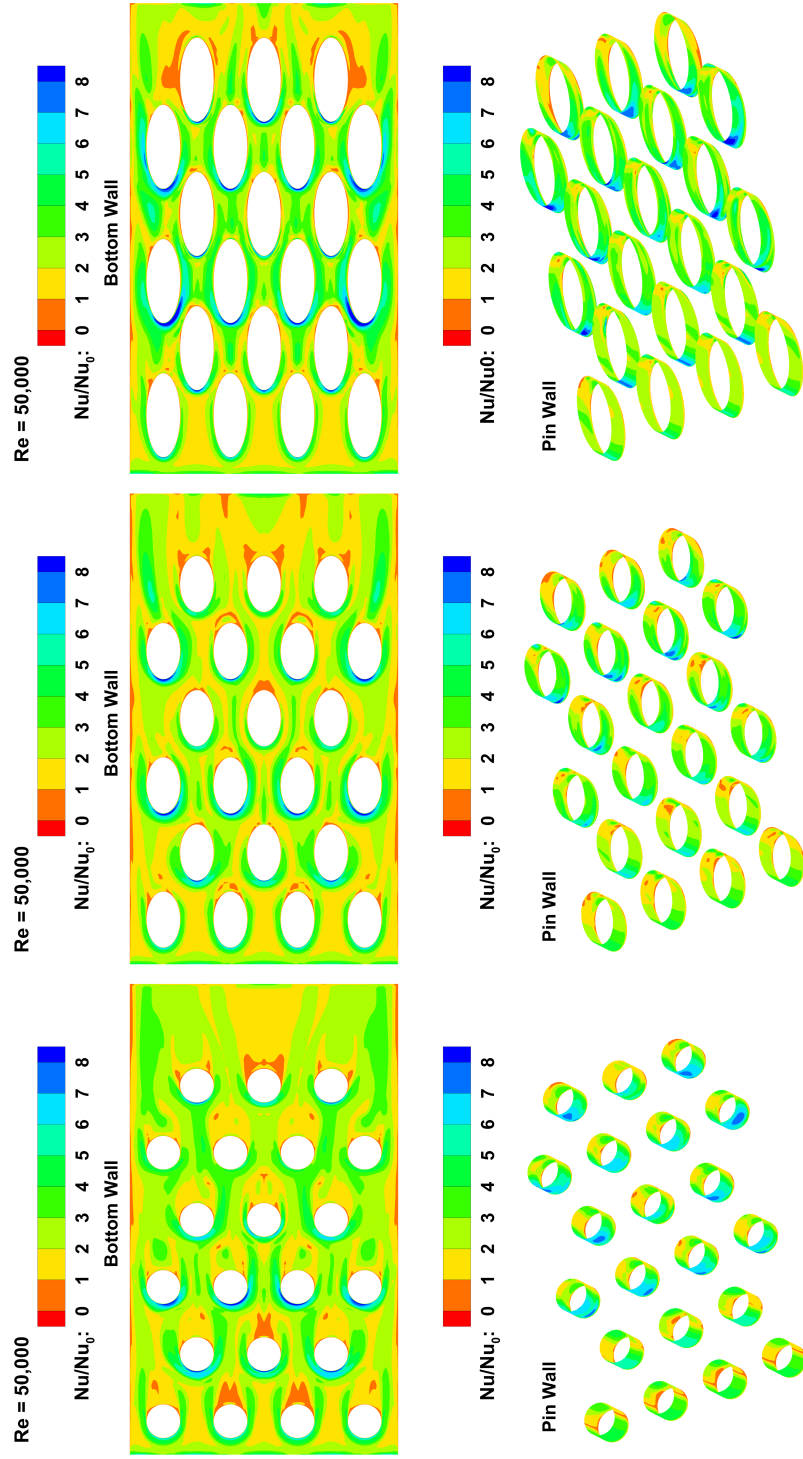Fig. 17. Contours of Nusselt number ratio on bottom wall and pin wall for circular, SEF and N fin arrays (Re=30,000)

Fig. 18. Contours of Nusselt number ratio on bottom wall and pin wall for circular, SEF and N fin arrays (Re=50,000)
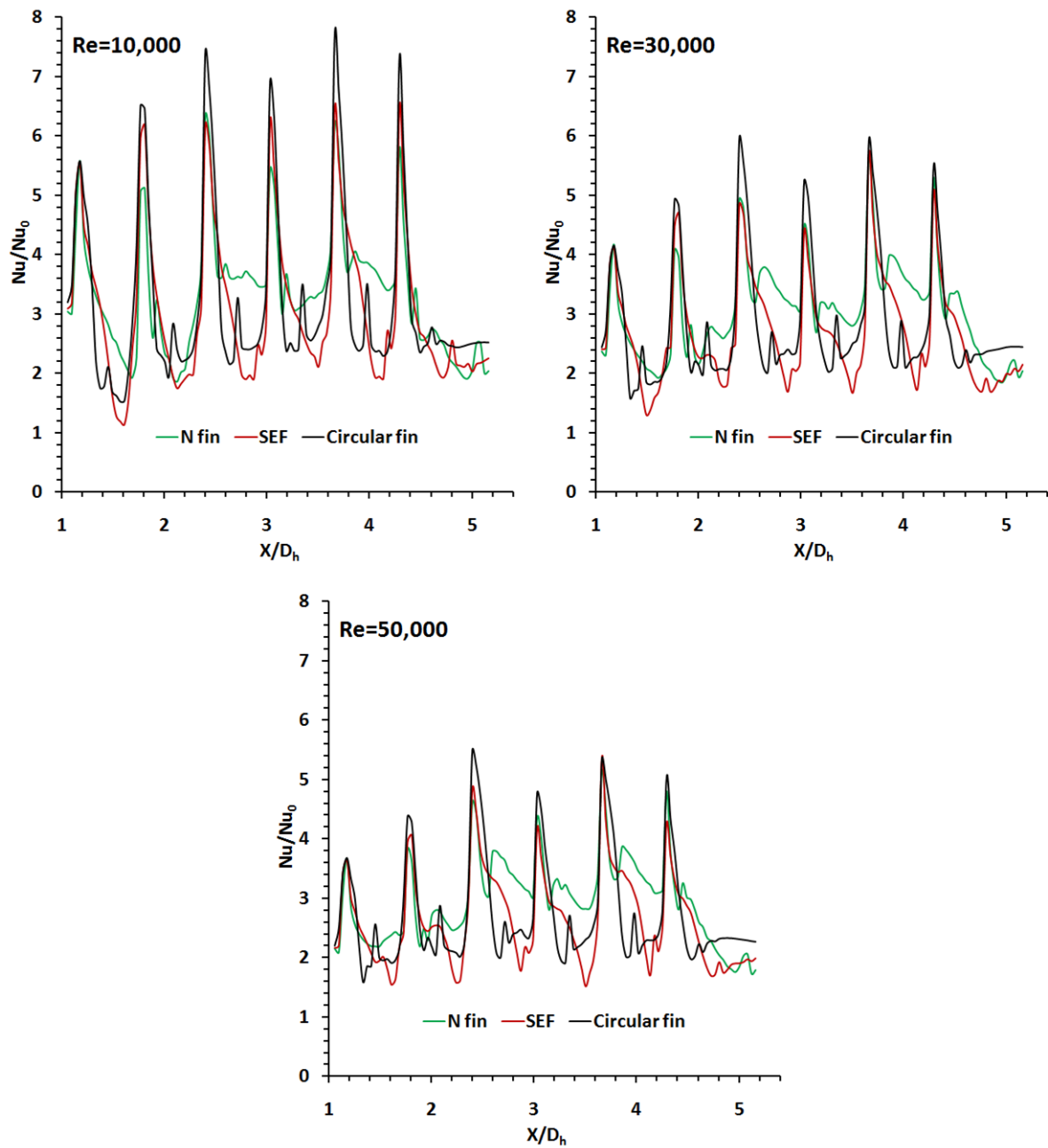
Fig. 19. Spanwise averaged Nusselt number ratio versus Reynolds number for circular, SEF and N fin arrays

pin wall combined together come down although the absolute Nu values increase. The above discussion on heat transfer is valid for all fin shapes with a few anomalies. For Re = 10,000 and 30,000, the maximum value of Nu/Nu_0 in the second row is lower than that of first row from Fig. 19. Interference of the low heat transfer wake region with the high heat transfer region in the second row reduces its maximum value of spanwise average of Nu/Nu_0 value but this low heat transfer wake region is absent in the first row. That is possibly the reason why this anomaly is absent in N fin array for Re = 50,000 where the size of the wake is significantly smaller than Re = 10,000 and 30,000. The following subsection lists the differences in the heat transfer patterns of the three fin shapes.

1. Effect of major axis length on heat transfer

As discussed in section E of Chapter III, the parameters "size of the wake" and "interaction between consecutive rows of pin fins" have similar effect on heat transfer enhancement and as the major axis length increases, the former decreases and latter increases. Fig. 19 shows that the maximum Nu/Nu_0 values are highest in circular fin array when compared to SEF and N fin arrays. This is probably because the wake sizes are largest in circular fin arrays. Fig. 19 also shows that the hot spots (regions with low Nu/Nu_0 values) are least in N fin array when compared to circular and SEF fin arrays. Possible reason behind this is that the interaction between consecutive rows of pin fins is highest in N fin array leading to a drastic reduction in regions with low velocity (refer to Figs. 11, 12, 13). Fig. 20 presents the Nu/Nu_0 contours on a single pin fin located in the middle of fourth row for Re = 50,000. The Nu/Nu_0 values increase from the bottom wall-pin wall junction to the midplane of symmetry-pin wall junction due to increase in the velocity of impingement. Also the contours clearly show that the Nu/Nu_0 values are more uniform in N fin compared to circular
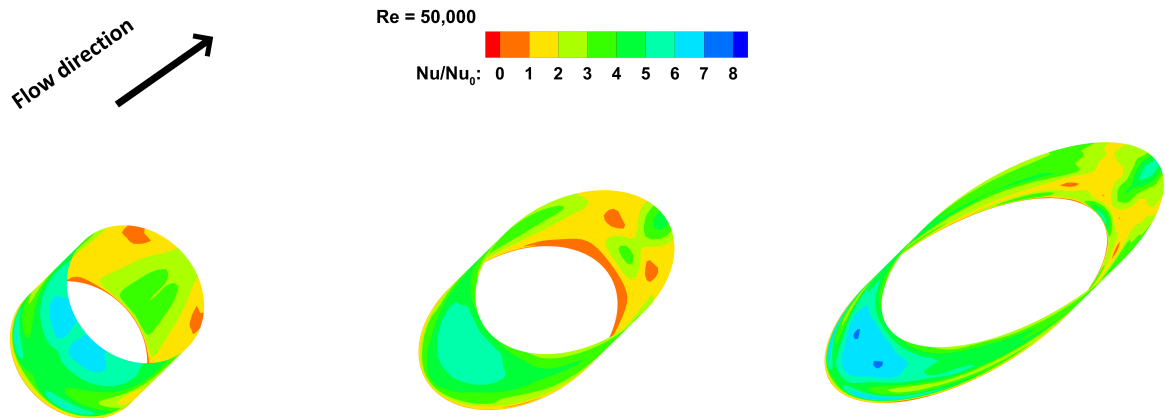
Fig. 20. Nusselt number ratio contours on a single pin fin in the middle of fourth row

fin and SEF. The combined effect of "size of the wake" and "interaction between consecutive rows of pin fins" parameters can be explained using Fig. 21 or Fig. 22 which present the channel averaged (spanwise average from the inlet of heated section to $0.5D$ downstream of the trailing edge of last pin fin row) Nu and Nu/Nu_0 values respectively plotted against Reynolds number. Circular and N fin arrays have similar Nu/Nu_0 values which are significantly higher than the values exhibited by SEF array. This is because one of "size of the wake" and "interaction between consecutive rows of pin fins" dominates in circular and N fin arrays whereas none of the parameters have a major effect in the case of SEF array. Another deduction worthwhile to be noted is that except for Re = 10,000, the channel averaged Nu/Nu_0 values of N fin array are slightly higher than that of circular fin array and the gap increases with Reynolds number. Probable reason behind this effect is the reduction in "size of the wake" but no reduction in "interaction between consecutive rows of pin fins" with increasing Reynolds number. Apart from that the channel averaged Nu values increase with Reynolds number from Fig. 21 for all fin shapes as expected due to
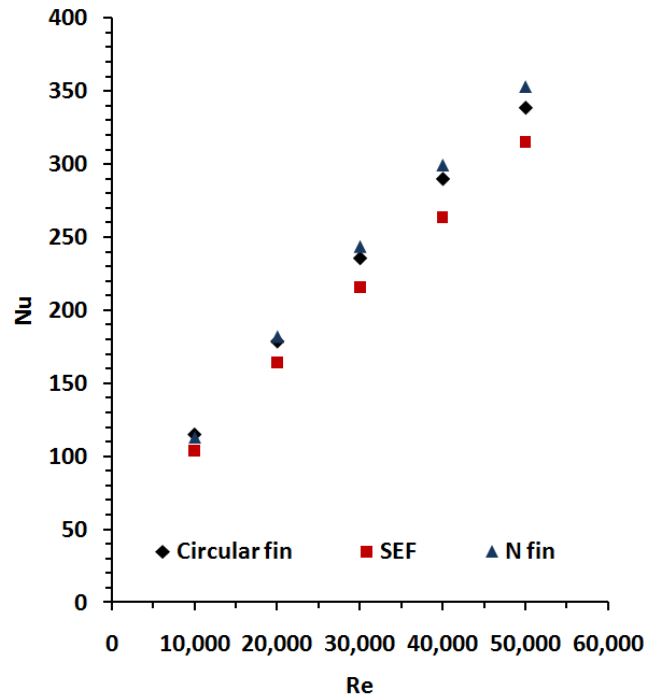
Fig. 21. Channel averaged Nusselt number versus Reynolds number for circular, SEF and N fin arrays

increase in turbulence whereas the Nu/Nu_0 values decrease with increase in Reynolds number from Fig. 22 which is to be expected as smooth duct Nusselt number (Nu_0) values show a sharp increase with Reynolds number.

H.   Thermal Performance

Addition of pin fins increases heat transfer at the cost of increase in pressure loss (which is directly related to pumping power). So it is necessary to compare the values of thermal performance (TP), a parameter to measure the profitability of using a particular cooling technique. The definition of thermal performance (TP) is
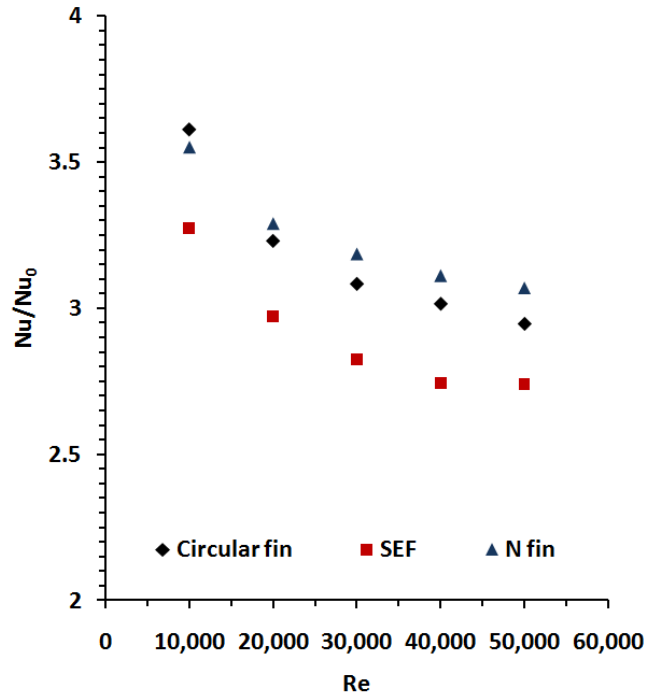
Fig. 22. Channel averaged Nusselt number ratio versus Reynolds number for circular, SEF and N fin arrays

as follows:

$$TP = \frac{\dfrac{\text{Nu}}{\text{Nu}_0}}{\left(\dfrac{f}{f_0}\right)^{1/3}} \tag{3.9}$$

Fig. 23 presents the TP values plotted against Re for all fin shapes. It is evident that SEF array has the highest TP values among the three fin shapes for all Re. Referring back to Figs. 15 and 22, although SEF array has the lowest Nu/Nu_0 values, it is compensated by much lower f/f_0 values leading to highest thermal performance. Second highest TP values are exhibited by N fin array which as shown in Fig. 22 produce the highest Nu/Nu_0 values excepting Re = 10,000. Another positive aspect about N fin array is the drastic reduction in the hot spots when compared to the other two fin shapes. Finally circular fin array produces the lowest TP values in Fig. 23
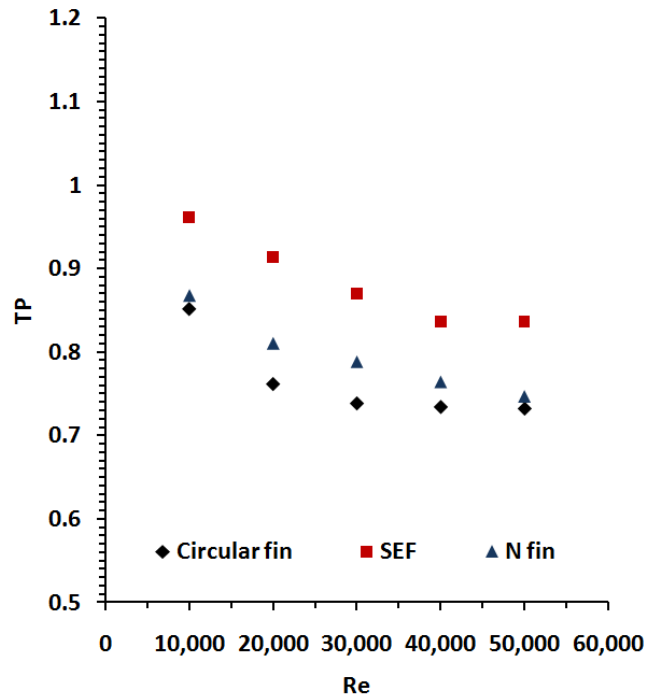
Fig. 23. Thermal performance (TP) variation with Reynolds number for circular, SEF and N fin arrays

for all Re. In addition to that, the hot spots and friction coefficient values (except Re = 50,000) are also the highest in circular fin array making it the least effective fin shape for cooling.

CHAPTER IV

SUMMARY AND CONCLUSIONS

The objective of current study was to numerically investigate the flow and heat transfer characteristics in a stationary one pass rectangular channel (AR=4:1) with circular and elliptical pin fin arrays. Two types of elliptical pin fins i.e., a SEF and an N fin whose minor axis length is equal to the diameter of the circular fin were used. The analysis was performed with an array of six rows of staggered pin fins in the streamwise direction for Reynolds numbers (Re) of 10,000, 20,000, 30,000, 40,000 and 50,000. 3-D, steady simulations were performed using the low Reynolds number k-omega SST turbulence model in the FLUENT CFD code. Circular pin fin array data were validated using Wright et al. [12] and Metzger et al. [6]. In order to test the ability of the current model to accurately predict data for SEF and N fin geometries, experiments performed by Camci and Uzol [22] on SEF and N fins were emulated and the numerical data were compared with experiments for Reynolds numbers (Re) 30,000, 40,000 and 50,000. Salient findings from this study are summarized below:

- The data predicted by the current numerical model showed good agreement with the experiments in the validation study.

- Velocity field: For all fin shapes, the flow mixed as it passed through the first two rows of pin fins, got sufficiently mixed by the third row and followed a roughly periodic pattern in the subsequent rows. It was observed that the size of the wake reduces as the major axis length increases for constant Reynolds number and also as the Reynolds number increases for constant major axis length. It was also observed that as the major axis length increases, the interaction between consecutive pin fin rows also increases as the spacing ratio is constant. Finally

the wakes of pin fins closest to the side wall in odd numbered rows in circular fin and SEF array were skewed towards the side wall but relatively straight in N fin array which indicates the higher interaction between pin fins and side wall in N fin array.

- Pressure loss: The friction coefficient (f) values decreased with increase in Reynolds number for constant major axis length for all fin shapes. Circular and N fin arrays showed similar friction coefficient values which were significantly higher than the values exhibited by SEF array. Also for Re = 10,000, circular fin array had slightly higher friction coefficient value when compared to N fin array and as the Reynolds number increased, the gap closed down and eventually the friction coefficient value of N fin array became more than that of circular fin array for Re = 50,000. Finally the friction coefficient ratio (f/f_0) values were almost independent of Reynolds number for SEF and N fin arrays and slightly dependant on Reynolds number for circular fin array.

- Similarities in heat transfer pattern: The spanwise averaged Nusselt number ratio (Nu/Nu_0) values increased in the first three rows and roughly periodic behaviour was shown by alternate rows subsequently. With increasing Reynolds number, channel averaged Nusselt number ratio values on the bottom wall and the pin wall combined together came down although the absolute Nusselt number values increased. For Re = 10,000 and 30,000, N fin array showed anomalous behaviour as the maximum value of spanwise averaged Nusselt number ratio in the second row was found to be lower than that of first row.

- Differences in heat transfer pattern: Maximum values of spanwise averaged Nusselt number ratio were highest in circular fin array when compared to SEF and N fin arrays. The hot spots (regions with low Nusselt number ratio) were

least in N fin array when compared to cirular fin and SEF arrays. Circular and N fin arrays showed similar channel averaged Nusselt number ratio values which were significantly higher than the values exhibited by SEF array. Except for Re = 10,000, the channel averaged Nusselt number ratio values of N fin array were slightly higher than that of circular fin array and the gap increased with Reynolds number.

- Thermal performance: SEF array had the highest Thermal performance (TP) values among the three fin shapes for all Reynolds numbers. Second highest Thermal performance values were exhibited by N fin array which also produced the highest channel averaged Nusselt number ratio values excepting Re = 10,000 (when the values were similar). Finally circular fin array produced the lowest Thermal performance values.

Cooling technique should be chosen based on the priorities of the application. If the priority is minimum pressure loss or highest thermal performance, then SEF array is the ideal choice. If having minimum hot spots or highest channel averaged Nusselt number ratio values is the priority, then N fin array is the ideal choice. Considering the better performance shown by SEF and N fin arrays, further investigation into them including channel rotation, varying spacing ratio, trapezoidal channel geometry, lateral flow ejection is necessary to understand their flow and heat transfer characteristics better and design superior cooling techniques.

REFERENCES

[1] J. C. Han, S. Dutta, and S. V. Ekkad, *Gas Turbine Heat Transfer and Cooling Technology*, New York: Taylor and Francis, 2000.

[2] M. Jakob, "Heat Transfer and Flow Resistance in Crossflow of Gases Over Tube Banks," *Trans. ASME*, vol. 60, pp. 384–386, 1938.

[3] E. D. Grimison, "Correlation and Utilization of New Data on Flow Resistance and Heat Transfer for Crossflow of Gases Over Tube Banks," *Trans. ASME*, vol. 59, pp. 583–594, 1937.

[4] G. J. VanFossen, "Heat Transfer Coefficients for Staggered Arrays of Short Pin Fins," *Trans. ASME J. Heat Transfer*, vol. 104, pp. 268–274, 1982.

[5] D. E. Metzger, R. A. Berry, and J. P. Bronson, "Developing Heat Transfer in Rectangular Ducts With Staggered Arrays of Short Pin Fins," *J. Heat Transfer*, vol. 104, pp. 700-706, 1982.

[6] D. E. Metzger, Z. X. Fan, and W. B. Shepard, "Pressure Loss and Heat Transfer Through Multiple Rows of Short Pin Fins," in *Proceedings of the 7th International Heat Transfer Conference*, Munich, Germany, Hemisphere Publishing Corp., vol. 3, pp. 137-142, 1982.

[7] J. Armstrong and D. Winstanley, "A Review of Staggered Array Pin Fin Heat Transfer for Turbine Cooling Applications," *ASME J. Turbomach.*, vol. 110, pp. 94-103, 1988.

[8] S. C. Lau, J. C. Han, and Y. S. Kim, "Turbulent Heat Transfer and Friction in Pin Fin Channels With Lateral Flow Ejection," *J. Heat Transfer*, vol. 111, pp. 51-58, 1989.

[9] D. E. Metzger, W. B. Shepard, and S. W. Haley, "Row resolved heat transfer variations in pin-fin arrays including effects of non-uniform arrays and flow convergence," in *International Gas Turbine Conference and Exhibit*, Dusseldorf, West Germany, ASME Paper No. 86-GT-132, 1986.

[10] J. J. Hwang and C. C. Lui, "Measurement of endwall heat transfer and pressure drop in a pin-fin wedge duct," *Int. J. Heat Mass Transfer*, vol. 45, pp. 877–889 , 2002.

[11] F. T. Willett and A. E. Bergles, "Heat transfer in rotating narrow rectangular pin-fin ducts," *Exp. Therm. Fluid Sci.*, vol. 25, pp. 573-582, 2002.

[12] L. M. Wright, E. Lee, and J. C. Han, "Effect of Rotation on Heat Transfer in Rectangular Channels with Pin Fins," *AIAA J. Thermophys Heat Transfer*, vol. 18, pp. 263–272, 2004.

[13] D. E. Metzger, C. S. Fan, and S. W. Haley, "Effects of pin shape and array orientation on heat transfer and pressure loss in pin fin arrays," *ASME J. Eng. Gas Turbines Power*, vol. 106, pp. 252–257, 1984.

[14] E. M. Sparrow and V. B. Grannis, "Pressure Drop Characteristics of Heat Exchangers Consisting of Arrays of Diamond-Shaped Pin Fins," *Int. J. Heat Mass Transfer*, vol. 34, pp. 589–600, 1991.

[15] V. B. Grannis and E. M. Sparrow, "Numerical simulation of fluid flow through an array of diamond-shaped pin fins," *Numer. Heat Transfer*, vol. 19, pp. 381–403, 1991.

[16] G. Tanda, "Heat transfer and pressure drop in a rectangular channel with diamond-shaped elements," *Int. J. Heat Mass Transfer*, vol. 44, pp. 3529–3541,

2001.

[17] M. K. Chyu, Y. C. Hsing, and V. Natarajan, "Convective Heat Transfer of Cubic Fin Arrays in a Narrow Channel," *ASME J. Turbomach.*, vol. 120, pp. 362–367, 1998.

[18] A. K. Saha and S. Acharya, "Unsteady simulation of turbulent flow and heat transfer in a channel with periodic array of cubic pin-fins," *Numer. Heat Transfer (Part A)*, vol. 46, pp. 731-763, 2004.

[19] R. J. Goldstein, M. Y. Jabbari and S. B. Chen, "Convective mass transfer and pressure loss characteristics of staggered short pin-fin arrays," *Int. J. Heat Mass Transfer*, vol. 37, pp. 149–160, 1994.

[20] Z. Chen, Q. Li, D. Meier, and H. J. Warnecke, "Convective Heat Transfer and Pressure Loss in Rectangular Ducts With Drop-Shaped Pin Fins," *Heat Mass Transfer*, vol. 33, pp. 219-224, 1997.

[21] Q. Li, Z. Chen, U. Flechtner, and H. J. Warnecke, "Heat Transfer and Pressure Drop Characteristics in Rectangular Channels With Elliptic Pin Fins," *Int. J. Heat Fluid Flow*, vol. 19, pp. 245-250, 1998.

[22] O. Uzol and C. Camci, "Heat Transfer, Pressure Loss and Flow Field Measurements Downstream of Staggered Two-Row Circular and Elliptical Pin Fin Arrays," *J. Heat Transfer*, vol. 127, pp. 458-471, 2005.

[23] FLUENT Inc., *FLUENT 12.0 Users Guide*, www.fluent.com, 2009.

APPENDIX A

NOMENCLATURE

AR = test section aspect ratio

D = circular fin diameter or SEF/N fin minor axis length, m

D_h = hydraulic diameter, m

f = friction coefficient

f_0 = friction coefficient in fully developed turbulent nonrotating tube flow

H = pin height or test section height, m

h = heat transfer coefficient, $q_w/(T_w - T_b)$, W/m²ºC

k = thermal conductivity of coolant, W/mºC

L_1 = unheated smooth starting section of the test section

L_2 = heated section of the test section

L_3 = unheated smooth exit section of the test section

Nu = local Nusselt number

Nu_0 = Nusselt number in fully developed turbulent nonrotating tube flow

Pr = Prandtl number

q_w = heat flux, W/m²

Re = Reynolds number

Re_D = array Reynolds number

S_1 = streamwise pin spacing, m

S_2 = spanwise pin spacing, m

T = local coolant temperature, ºC

T_b = local bulk mean temperature, ºC

T_o = inlet coolant temperature, ºC

T_w = local wall temperature, °C

V_m = mean velocity at the inlet of test section, m/s

V_{max} = mean velocity at minimum flow area, m/s

W = test section width, m

X = streamwise distance, m

X_1 = streamwise spacing between inlet of heated section and leading edge of first row pin fin, m

μ = dynamic viscosity of coolant, kg/m.s

ρ = density of coolant, kg/m^3

$\Delta\rho/\rho$ = inlet coolant-to-wall density ratio, $(T_w - T_o)/T_w$

VITA

Abhishek Velichala received his Bachelor of Technology degree in Mechanical Engineering from Indian Institute of Technology, Madras, India in July, 2008. He started his Master of Science program in Mechanical Engineering at Texas A&M University in Fall, 2008. The author may be contacted at Department of Mechanical Engineering, 3123 TAMU, College Station, TX 77843-3123 or by email at abhishek.v.iitm@gmail.com

The typist for this thesis was Abhishek Velichala.